

Document Version

Final published version

Licence

CC BY

Citation (APA)

Rouillon, C., Eckhardt, B. V., Kollenstart, L., Gruss, F., Verkennis, A. E. E., Rondeel, I., van Laar, T., Albanese, P., Dekker, N. H., & More Authors (2023). CAF-1 deposits newly synthesized histones during DNA replication using distinct mechanisms on the leading and lagging strands. *Nucleic Acids Research*, 51(8), 3770-3792. <https://doi.org/10.1093/nar/gkad171>

Important note

To cite this publication, please use the final published version (if applicable). Please check the document version above.

Copyright

In case the licence states "Dutch Copyright Act (Article 25fa)", this publication was made available Green Open Access via the TU Delft Institutional Repository pursuant to Dutch Copyright Act (Article 25fa, the Taverne amendment). This provision does not affect copyright ownership. Unless copyright is transferred by contract or statute, it remains with the copyright holder.

Sharing and reuse

Other than for strictly personal use, it is not permitted to download, forward or distribute the text or part of it, without the consent of the author(s) and/or copyright holder(s), unless the work is under an open content license such as Creative Commons.

Takedown policy

Please contact us and provide details if you believe this document breaches copyrights. We will remove access to the work immediately and investigate your claim.

CAF-1 deposits newly synthesized histones during DNA replication using distinct mechanisms on the leading and lagging strands

Clément Rouillon^{1,†}, Bruna V. Eckhardt^{1,†}, Leonie Kollenstart^{2,3,†}, Fabian Gruss¹, Alexander E.E. Verkennis¹, Inge Rondeel¹, Peter H.L. Krijger⁴, Giulia Ricci¹, Alva Biran^{2,3}, Theo van Laar⁵, Charlotte M. Delvaux de Fenffe¹, Georgiana Luppens¹, Pascal Albanese⁶, Koichi Sato⁴, Richard A. Scheltema⁶, Wouter de Laat⁴, Puck Knipscheer^{4,7}, Nynke H. Dekker⁵, Anja Groth^{2,3,*} and Francesca Mattioli^{1,*}

¹Hubrecht Institute-KNAW & University Medical Center Utrecht, Utrecht, The Netherlands, ²Novo Nordisk Foundation Center for Protein Research (CPR), University of Copenhagen, Copenhagen, Denmark, ³Biotech Research and Innovation Center, University of Copenhagen, Copenhagen, Denmark, ⁴Oncode Institute, Hubrecht Institute-KNAW and University Medical Center Utrecht, Utrecht, the Netherlands, ⁵Kavli Institute of Nanoscience Delft, TU Delft, The Netherlands, ⁶Utrecht Institute for Pharmaceutical Sciences, Utrecht University, the Netherlands and ⁷Department of Human Genetics, Leiden University Medical Center, Leiden, The Netherlands

Received August 09, 2022; Revised February 18, 2023; Editorial Decision February 22, 2023; Accepted February 23, 2023

ABSTRACT

During every cell cycle, both the genome and the associated chromatin must be accurately replicated. Chromatin Assembly Factor-1 (CAF-1) is a key regulator of chromatin replication, but how CAF-1 functions in relation to the DNA replication machinery is unknown. Here, we reveal that this crosstalk differs between the leading and lagging strand at replication forks. Using biochemical reconstitutions, we show that DNA and histones promote CAF-1 recruitment to its binding partner PCNA and reveal that two CAF-1 complexes are required for efficient nucleosome assembly under these conditions. Remarkably, in the context of the replisome, CAF-1 competes with the leading strand DNA polymerase epsilon (Pol ϵ) for PCNA binding. However, CAF-1 does not affect the activity of the lagging strand DNA polymerase Delta (Pol δ). Yet, in cells, CAF-1 deposits newly synthesized histones equally on both daughter strands. Thus, on the leading strand, chromatin assembly by CAF-1 cannot occur simultaneously to DNA synthesis, while on the lagging strand these processes may be coupled. We propose that these differences may facilitate distinct parental histone recycling mechanisms and accommodate the inherent asymmetry of DNA replication.

INTRODUCTION

During every cell cycle, a new copy of the genome is made. At the same time, genomic chromatin organization must be replicated to ensure faithful transmission of the parental epigenetic state to both daughter cells after cell division. Therefore, genome and chromatin replication are tightly coupled and regulated by the concerted action of several dozens of proteins. Errors in both processes affect cell function; they can derail developmental programs or cause diseases, such as cancer (1–4).

DNA is replicated by the replisome, which is comprised of a core Cdc45-MCM-GINS (CMG) helicase complex, DNA polymerases and regulatory factors (5–9). Two distinct DNA polymerases function on the two daughter strands: DNA polymerase epsilon (Pol ϵ) acts on the leading strand, whereas DNA polymerase delta (Pol δ) acts on the lagging strand (10–14). Because both DNA polymerases synthesize DNA in the 5′–3′ direction, the two strands are replicated via distinct mechanisms. Pol ϵ tightly binds the CMG and continuously extends the leading strand, while Pol δ discontinuously synthesizes short Okazaki fragments, which are later processed and ligated on the lagging strand (13–17). Despite their mechanistic differences, both DNA polymerases require the processivity factor Proliferating Cell Nuclear Antigen (PCNA) for their function. PCNA is an essential homotrimeric clamp that encircles newly synthesized double-stranded DNA, tethering the DNA polymerases to DNA. It is abundant at replication forks where,

*To whom correspondence should be addressed. Tel: +31 30 212 1800; Email: f.mattioli@hubrecht.eu
Correspondence may also be addressed to Anja Groth. Email: anja.groth@cpr.ku.dk

[†]The authors wish it to be known that, in their opinion, the first three authors should be regarded as Joint First Authors.

in addition to the DNA polymerases, it binds many other factors involved in genome replication, chromatin assembly and the response to stress and damage (18–20).

Chromatin replication requires proteins that function as histone chaperones, which include replisome components with histone binding properties (i.e. MCM2, Pole, Pol α and RPA) and *bona fide* histone chaperones that are recruited to the replisome (i.e. FACT, CAF-1 and ASF1) (4). These proteins coordinate the recycling of parental histones to spatially maintain the landscape of histone post-translational modifications. They also promote the incorporation of newly synthesized histones to preserve nucleosome density on the daughter DNA strands (2,4). Replicated DNA is readily assembled into chromatin (21,22), a process that constitutes the first critical step to the re-establishment of epigenetic modifications on histones genome-wide (2,4,23–27).

Chromatin Assembly Factor-1 (CAF-1) is a key regulator of chromatin assembly during DNA replication (28). CAF-1 deletion is lethal during vertebrate development (29–31), and transient CAF-1 depletion affects cell cycle progression and cell fate (26,32–41). CAF-1 forms a heterotrimeric complex consisting of Cac1, Cac2 and Cac3 in yeast and p150, p60 and p48 in mammals. The complex chaperones newly synthesized histones H3–H4 and deposits them onto DNA at sites of DNA synthesis (42–47). CAF-1 activity at replication forks depends on its interaction with PCNA, which occurs via canonical PCNA Interacting Peptides (PIPs) present on the large CAF-1 subunit (48–53). While the function of CAF-1 has been studied in cells and in the SV40 systems, a detailed bottom-up biochemical reconstitution to address the molecular mechanism by which CAF-1 assembles chromatin during DNA replication and its interplays with the replisome is still lacking.

Here we developed biochemical systems to study the crosstalk between CAF-1 and key components of the DNA replication machinery, combining our previous CAF-1 histone chaperone assays (54,55) with primer extension assays and the recent *in vitro* reconstitution of the eukaryotic replisome (8,9). We find that CAF-1 recruitment to PCNA requires DNA and is modulated by histones. Two CAF-1 complexes bind PCNA and are necessary for PCNA-dependent nucleosome assembly. CAF-1 interaction with PCNA inhibits the activity of the leading-strand DNA polymerase Pole, but not of the lagging-strand polymerase Pol δ . Yet, in cells, we show that CAF-1 deposits histones equally on the leading and lagging strands during DNA replication. Thus, our work reveals an unexpected difference in the crosstalk between CAF-1, PCNA and the two replicative polymerases, suggesting different mechanisms for the coupling of nucleosome assembly to DNA synthesis on the two daughter strands.

MATERIALS AND METHODS

Protein expression and purification

CAF-1 and PCNA mutants were made using standard mutagenesis procedures and purified following the wild-type purification protocols. We used yeast proteins, with the exception of *Xenopus laevis* histones and FEN1. Several proteins used in our study were expressed and purified as

previously described. This includes PCNA (56), Pol δ and Pole (8,9), CAF-1 and its mutants (54). Lyophilized *X. laevis* histones were purchased from the Histone Source at CSU, Fort Collins, CO, USA. These were labeled with maleimide dyes (when required) and refolded as in (57,58). ORC, cdc6, Mcm2/7-cdt1, DDK, cdc45, Dpb11, GINS, S-CDK, Mcm10, RPA, Pol α , Ctf4, Sld3/7, Sld2 and TopoII were purified as in (8). Csm3/Tof1, Topo I, RFC and PCNA were purified as described in (9). Mrc1 was expressed and purified following the procedure described in (59). PCNA-C4S-K164C from Zhihao Zhuang (60) does not contain a His-tag and it was purified with two HiTrapQ rounds of purification before gel filtration. All the concentrations for PCNA reported here refer to the monomer concentration. Additional purification protocols are:

RFC Δ N. Rosetta2 cells containing pBL481-RFC Δ N from Peter Burgers (61) were grown in 4 liters of Terrific Broth at 37°C to $A_{600} = 1.6$. The temperature was shifted to 18°C and cells were incubated for 30 more min before adding 0.3 mM isopropyl-thiogalactoside (IPTG). The expression was incubated for 16 h and cells were harvested and resuspended in 30 mM HEPES pH 7.5, 0.5 mM EDTA, 10% glycerol, 200 mM NaCl, 1 mM DTT, 0.5 mM *p*-methylphenyl-sulfonyl fluoride (PMSF) in presence of COMPLETE EDTA-free protease inhibitor (Roche). Cells were lysed with sonication. DNA was precipitated with 0.5% of poly(ethyleneimine) (PEI) and the lysate was clarified by centrifugation for 30 min at 35000xg. RFC Δ N was precipitated with 0.28 g/ml of AmSO $_4$. The precipitates were collected by centrifugation at 12 000 xg for 45 min. Pellets were resuspended in 50 ml of 30 mM HEPES pH 7.5, 0.5 mM EDTA, 10% glycerol + 1 mM DTT, 0.5 mM PMSF in presence of COMPLETE EDTA-free protease inhibitor. The lysate was next dialyzed (12–14 MWCO) against 2 liters of 30 mM HEPES pH 7.5, 0.5 mM EDTA, 10% glycerol + 100 mM NaCl, 1 mM DTT for 2 h. RFC Δ N was injected on HiTrap SP HP 5ml column (Cytiva) equilibrated in buffer SP-A (30 mM HEPES pH 7.5, 10% glycerol, 100 mM NaCl, 1 mM TCEP). The column was washed with 25 ml of SP-A buffer and RFCN was eluted in a gradient of SP-B buffer (30 mM HEPES pH 7.5, 10% glycerol, 800 mM NaCl, 1 mM TCEP) along 60 ml. Fractions containing RFC Δ N were analyzed by SDS-PAGE and were pooled together. RFC Δ N was then mixed with 3 ml of nickel beads equilibrated in His-A buffer (20 mM HEPES 7.5, 200 mM NaCl, 20 mM imidazole, 10% glycerol, 1 mM TCEP). Beads were washed with 100 ml of His-A buffer and RFC Δ N was eluted with His-B buffer (20 mM HEPES 7.5, 300 mM NaCl, 300 mM imidazole, 10% glycerol, 0.05% ampholytes, 1 mM TCEP). Fractions containing RFC were concentrated and further purified on HiLoad 16/600 Superdex 200 in 20 mM HEPES 7.5, 200 mM NaCl, 10% glycerol, 1 mM TCEP, 0.05% ampholytes. RFC Δ N was concentrated and stored at –80°C.

RPA from bacterial expression. Rosetta2 cells transformed with pRSF-Duet, RPA, a gift from Xiaodong Zhang (62), were grown in 2 liters of Terrific Broth at 37°C for 16 h until $A_{600} = 1.8$. Cells were placed at 25°C and RPA expres-

sion was induced with 0.3 mM IPTG for 3 h. Cells were harvested and resuspended in lysis buffer (50 mM HEPES pH 7.5, 500 mM NaCl, 5% glycerol, 0.01% IGEPAL CA-630, 1 mM TCEP) in presence of COMPLETE EDTA-free protease inhibitor (Roche). Cells were sonicated and the lysate was clarified by centrifugation at 50 000×g for 50 min. The supernatant was recovered and injected on His-Trap HP 5 ml column equilibrated in lysis buffer. The column was washed with 50 ml of lysis buffer, 100 ml of His-A buffer (50 mM HEPES pH 7.5, 750 mM NaCl, 5% glycerol, 0.01% IGEPAL CA-630, 1 mM TCEP, 30 mM imidazole), and 25 ml of lysis buffer respectively. RPA was then eluted in a gradient of His-B buffer (50 mM HEPES pH 7.5, 150 mM NaCl, 5% glycerol, 0.01% IGEPAL CA-630, 1 mM TCEP, 250 mM imidazole) along 50 ml. Fractions containing RPA were pooled and diluted in 50 mM HEPES pH 7.5, 5% glycerol, 0.01% IGEPAL CA-630, 1 mM TCEP to bring the salt concentration to 150 mM NaCl. RPA was next injected on HiTrap Heparin HP 1 ml equilibrated in QA buffer (50 mM HEPES pH 7.5, 150 mM NaCl, 5% glycerol, 0.01% IGEPAL CA-630, 1 mM TCEP). The column was washed with 20 ml of QA buffer and RPA was eluted in a gradient of QB buffer (50 mM HEPES pH 7.5, 1000 mM NaCl, 5% glycerol, 0.01% IGEPAL CA-630, 1 mM TCEP) along 40 ml. Fractions containing RPA were pooled together and injected on HiLoad 16/600 Superdex 200 and eluted in 50 mM HEPES pH 7.5, 300 mM NaCl, 5% glycerol, 0.01% IGEPAL CA-630, 1 mM TCEP. RPA was concentrated and stored at -80°C .

FEN1_{DA} from bacterial expression. The cDNA encoding the full-length *X. laevis* FEN1 (S-form) D181A mutant was codon-optimized, synthesized (gBlocks Gene Fragments, Integrated DNA Technologies), and ligated into the BamHI–XhoI sites of the pGEX6P-1 vector. BL21 (DE3) RIL cells transformed with pGEX6P-1-xlFEN1.S_{DA} were grown in 2.4 l of LB + ampicillin at 30°C until $A_{600} = 0.7$. Cells were placed at 18°C and FEN1_{DA} expression was induced with 0.5 mM IPTG for overnight. Cells were harvested and resuspended in 40 ml lysis buffer (50 mM Tris–HCl pH 8, 500 mM NaCl, 10% glycerol, 1 mM EDTA, 1 mM PMSF, 0.1% IGEPAL CA-630, 2 mM DTT) in presence of COMPLETE EDTA-free protease inhibitor (Roche). Cells were sonicated and the lysate was clarified by centrifugation at 26 500×g for 20 min. The supernatant was recovered and added to Glutathione Sepharose 4B beads (Cytiva) equilibrated in lysis buffer. After incubation for 90 min, the beads were washed with 100 ml of wash buffer 1 (50 mM Tris–HCl pH 8, 1 M NaCl, 10% glycerol, 1 mM EDTA, 1 mM PMSF, 0.1% IGEPAL CA-630, 2 mM DTT). Washed the beads with 50 mL wash buffer 2 (50 mM Tris–HCl pH 8, 300 mM NaCl, 10% glycerol, 0.1% IGEPAL CA-630, 2 mM DTT). Beads were resuspended in 2 ml wash buffer 2 and RPA was cleaved from the beads overnight at 4°C using 100 U PreScission protease. Concentrated FEN1_{DA} was injected on Superose 6 Increase 10/300 GL (Cytiva) and eluted in Superose 6 buffer (20 mM HEPES–KOH pH 7.4, 300 mM NaCl, 10% glycerol, 2 mM DTT). Fractions were selected and FEN1_{DA} was concentrated and stored at -80°C .

Protein labelling with fluorescent dyes

Histones H2A–H2B (containing H2B-T112C) and H3–H4 (containing H4-E63C) were labeled with maleimide AlexaFluor-647 (AF647) or AlexaFluor-488 (AF488) respectively (57,58), as indicated.

PCNA-C4S-K164C and PCNAK164C were labeled with Alexa Fluor 546. PCNA was diluted in labelling buffer (50 mM MOPS pH 7.0, 125 mM NaCl, 5 mM NaAc, 1 mM EDTA, 1 mM TCEP) to a final concentration of 1 mg/ml. A 10-fold excess of TCEP was added to PCNA to ensure that all cysteines are effectively reduced. PCNA was then incubated with a 10-fold excess of AlexaFluor546. The reaction was incubated for 2 h at room temperature, then quenched with 20 mM DTT final concentration for 30 min. Labelled PCNA was then concentrated and injected on a Superdex 75 increase 10/300 column to remove free dyes. PCNA was eluted in 20 mM HEPES pH 7.5, 125 mM NaCl, 1 mM TCEP. Fractions containing labelled PCNA were pooled and concentrated, and the protein was stored at -80°C .

Annealing of linear DNA fragments

Single-stranded DNA oligos of different lengths were purchased from IDT, either desalted (unlabeled oligos) or HPLC-purified (Alexa Fluor 647-conjugated oligos). For each length (18mer, 33mer, 43mer, 53mer) a forward oligo and a reverse oligo in reverse complement sequence were ordered. The 18mer and 33mer forward oligos included a 5' Alexa Fluor 647 label. Forward and corresponding reverse oligos were mixed in a 1:1 stoichiometric ratio at 20 μM each (18mer and 33mer) or 40 μM each (43mer and 53mer) with a final of 20 mM HEPES pH 7.5 and 25 mM NaCl. The mixed oligos were annealed by heating up to 95°C for 3 min, and then slowly cooled to room temperature over several hours. Annealed DNA was stored at -20°C .

EMSA

Native DNA-protein complexes were allowed to form in NA buffer: 25 mM Tris pH 7.5, 150 mM NaCl, 1 mM EDTA, 0.02% Tween-20, 1 mM TCEP. Increasing amounts of CAF-1 (0–5 μM) were incubated in buffer for 10 minutes before addition of DNA (50 nM). Single stranded DNA oligos for 18, 33, 43 or 53 bp were purchased from IDT (labelled with AlexFluor647 at their 5' end, Supplementary Table S1) and annealed prior to the EMSA experiments. 10% final concentration of glycerol was added before loading the samples into a 6% PAGE. Gels were scanned for fluorescence and then stained with SybrGOLD before imaging with Amersham Image Quant 800. The data was analyzed and plotted using FIJI and GraphPad Prism. We quantified the fluorescent signal of the unbound DNA band. We calculate the percentage of unbound DNA relative to the no CAF-1 condition. %bound DNA is then expressed as 100 – percentage of unbound DNA. The K_d values were calculated using a one site binding curve with hill slope in GraphPad Prism. The 18bp data was fitted to a one site binding curve with a Hill coefficient constrained to 1.

PCNA-CAF-1 binding experiments on SEC

We used pUC19 plasmid as DNA template for PCNA loading. This plasmid was nicked using the restriction enzyme Nt.BspQI for 8 h at 50°C, and was subsequently purified via phenol chloroform extraction. Reactions were performed in PCNA loading buffer 50 mM HEPES pH 7.5, 200 mM NaCl, 0.01% IGEPAL CA-360, 1mM TCEP. PCNA (30 μM) was incubated for 5 min at 30°C with nicked pUC19 (0.3 μM) and RFCΔN (0.5 μM), in the presence of MgCl₂ (10 mM) and ATP (3 mM). Next, CAF-1 (5 μM) was added to these reactions and incubated for 15 min at room temperature. Samples were next spun down for 5 min at 17 000×g before injection on Superose 6 increase 3.2–300 columns connected to an AKTA pure system fitted with PEEK I.D. 0.25 mm tubing. The column was equilibrated in PCNA loading buffer supplemented with 10 mM MgCl₂. Fractions were analyzed on 4–12% gradient SDS-PAGE run in MES buffer.

PCNA-NAQ assay

We used pRC1765 (Addgene #141346, a gift from Rafael Fernández Leiro) as template for PCNA loading and nucleosome assembly. pRC1765 was nicked using the restriction enzyme Nt.BbvCI for 6 h at 37°C, and was subsequently purified via phenol chloroform extraction. PCNA was loaded on DNA in PCNA loading buffer, in a final volume of 11 μl: PCNA (10.9 μM) was added to an equimolar mixture of nicked and supercoiled pRC1765 (47.3 nM each), RFCΔN (1.1 μM) in presence of MgCl₂ (8 mM) and ATP (10.9 mM). This reaction was incubated at 30°C for 5 min. Then, samples were diluted with 25 μl of NA buffer in order to decrease the high concentration of MgCl₂ which hinder proper nucleosome assembly, followed by addition of CAF-1•H3–H4 (0.1 μM final concentration for each—H3–H4 dimer concentration) to a final volume of 40 μl total. This tetrasome assembly step was incubated at room temperature for 15 min. Then, we added fluorescently labelled H2A–H2B dimers (0.1 μM) and incubated for 15 min at room temperature, to complete nucleosome formation (63). Samples were spun down for 5 min at 17 000×g. 1 μl of each reaction was mixed with 5 μl of NA buffer and 5% sucrose final concentration for loading on 0.8% agarose gel and run for 90 min in 1× TAE (Tris-Acetate EDTA) at 90 V. 25 μl of each reaction was digested with 80 units of MNase in a total volume of 100 μl (containing 50 mM Tris pH 7.9, 5 mM CaCl₂) at 37°C for 10 min. MNase was inactivated by addition of EDTA. A 621 bp DNA fragment was added as loading control and the DNA was further purified as in (63). MNase-digested samples were loaded on 6% PAGE and stained with SybrGOLD. The data was analyzed and plotted using FIJI, and GraphPad Prism. The PCNA-mediated activity of CAF-1 is quantified as the percentage of fluorescence on nicked plasmid relative to the total intensity (nicked + supercoiled) for each condition. The amount of MNase-protected fragments in each condition was quantified using Bioanalyzer (Agilent) on DNA High sensitivity chips. The bioanalyzer data was analyzed by normalizing the nucleosome band (140–160 bp) to the loading control at 621 bp within each lane, as in (63). Data was then plotted using GraphPad Prism.

MNase-seq of PCNA-NAQ assay

MNase-seq was used to quantify nucleosome assembly in the PCNA-NAQ assay. In order to distinguish nucleosomes made on nicked and supercoiled DNA, we used two plasmids with different sequences: pRS415 and pLox3 (Supplementary Table S2). After MNase inactivation a 207 bp DNA fragment was added as loading control in these experiments. Purified MNase-digested products (containing the loading control DNA) were used to prepare a Illumina sequencing library. First, samples were purified using the CleanNGS kit (GC biotech #CNGS-0008), according to the manufacturer's protocol. Next, the CleanNGS elute was adjusted to 25ul with 10mM Tris pH 7.5 and the ends of the digested DNA were repaired and phosphorylated at their 5' end using the End-It DNA End-repair kit (Lucigen #ER0720). DNA was purified using MinElute PCR Purification Kit (QIAGEN #28006). Next, 3'A overhang were added to each fragment using the Klenow fragment (NEB #M0212M) and DNA was purified using MinElute PCR Purification Kit (QIAGEN #28006). Next, unique indexed DNA adapters (Supplementary Table S3) were ligated overnight at room temperature to all fragments with A-overhangs using T4 DNA ligase (NEB # M0202L). DNA was purified using MinElute PCR Purification Kit (QIAGEN #28006). Finally, all samples were amplified by a 8-cycles PCR-program using Phusion High-Fidelity DNA Polymerase (NEB #M0530L) using primers 5'-TCGTCGGCAGCGTCAGATGTGTATAAGAGACA GCTCGGCATTCTGCTGAACCGCTCTTCCGAT CT-3' and 5'-GTCTCGTGGGCTCGGAGATGTGTA TAAGAGACAGTACACTCTTCCCTACACGACG CTCTTCCGATCT-3', prior to a final clean up using the MinElute Purification Kit (QIAGEN #28006). Samples were pooled with a total concentration of 100 ng. The library was submitted for paired-end Illumina 150 bp PE sequencing at MacroGen (Amsterdam). fastq files are uploaded to OSF (https://osf.io/2vd4z/?view_only=5ffa1e0b749445da9b22a11577f3d47f). PCNA-NAQ-seq analysis was performed using custom scripts (<https://github.com/deLaatLab/PCNA-NAQ-seq>). The sequence data was demultiplexed by extracting reads that contained the ligated adapter index in both read ends and trimmed by removal of the 5' adapter sequence from the reads. Demultiplexed reads were mapped against the pLox3, pRS415 and loading control DNA sequences using BWA mem v0.7.17 and filtered using samtools with SAM flag 780 and mapping quality 60 and saved as bam files. The bam files were imported in R and fragments mapping to pLox3 and pRS415 with fragment lengths between 125 and 160 bp were selected for further analysis. The percentage of reads mapping to the nicked plasmid was calculated based on the total amount of reads found on both nicked and supercoiled plasmids. For coverage analysis pLox3 and pRS415 fragments were normalized for the total number of fragments mapping to the loading control sequence.

Primer extension assays

Experiments with Pole were performed in 25 mM HEPES–KOH pH 7.5, 150 mM potassium acetate, 8 mM MgAc₂, 1 mM TCEP, 1 mM ATP and 0.2 mg/ml BSA. Experiments

with Pol δ were performed in 25 mM Tris–HCl pH 7.5, 150 mM NaCl, 8 mM MgCl₂, 1 mM TCEP, 1 mM ATP and 0.2 mg/ml BSA. We used single stranded plasmid DNA as template for DNA synthesis, and it was produced as previously described (64). The concentrations reported here are for the final reaction that contains all components.

Single-strand pBluescript SK(-) (Supplementary Table S4) was incubated for 5 min at 80°C with a 5× excess of a 15 bp oligonucleotide and allowed to slowly cool down. The primer sequence is: G*G*G* T*T*C*GTGCACACA conjugated to an Alexa Fluor 647 dye at the 5' end (* indicates nucleotides containing phosphorothioate bonds). The annealing reaction was coated with RPA (0.6–1.5 μ M) for 5 min at 30°C. Next, PCNA (0.48 μ M) was loaded in presence of RFC Δ N (0.12 μ M) for 5 min at 30°C on DNA (12 nM). Pole or Pol δ (0.12 μ M) were primed onto the primer-template DNA in presence of dCTP, dGTP and dATP (75 μ M of each) for 5 min at 30°C. Finally, dTTP (75 μ M) was added to start the reaction. CAF-1 or FEN1 were also added at this step, at 300 nM unless stated otherwise in the figures. Reactions were quenched at various timepoints with 10 mM EDTA final concentration. Samples were mixed with 2% sucrose, 100 mM NaOH final concentrations and were loaded on denaturing alkaline 1.2% agarose gel. Gels were run for 16 h at 40V, and imaged on a Typhoon. The data was analyzed and plotted using FIJI, and GraphPad Prism. DNA synthesis is quantified as the intensity of the full-length plasmid band relative to the total intensity in the entire lane.

Primer extension assays performed in the presence of histones contained 180 nM of H3–H4 dimers added with CAF-1, Pole, or Pol δ . H2A–H2B dimers (180 nM) were added just before MNase digestion. For MNase analysis, 30 μ l of primer extension reactions at the final time point (16 min for Pole and 4 min for Pol δ) were mixed with 80 U of MNase in a total of 100 μ l (containing 50 mM Tris pH 7.9, 5 mM CaCl₂) at 37°C for 10 min. MNase was inactivated by addition of EDTA. A 621bp DNA fragment was added as loading control and the DNA was further purified as in (63). MNase-digested samples were loaded on 6% PAGE and stained with SybrGOLD and run on a Bioanalyzer (Agilent) using DNA High sensitivity chips. The bioanalyzer data was analyzed by normalizing the nucleosome band (140–150 bp) to the loading control at 621 bp within each lane, as in (63). Data was then plotted in excel and GraphPad Prism.

In-solution crosslinking experiments

CAF-1–PCNA on nicked plasmid. To buffer containing 20 mM HEPES pH 7.5, 200 mM NaCl, 1 mM TCEP, the following components were added in order at room temperature: 10 mM MgCl₂ (from 100 mM stock), 3 μ M PCNA K164C, 0.15 μ M RFC Δ N, 0.3 μ M nicked (with Nt.BspQ1) pUC19 plasmid (from 1 μ M stock), 1 mM ATP. This mixture was incubated at 30 °C for 5 min to increase the efficiency of PCNA loading onto DNA. Then, 1.5 μ M CAF-1 was added and incubated for 10 min at room temperature. The total NaCl concentration during the loading reaction and after adding CAF-1, taking into account the contributions from each component, ranged between 100 and 110

mM. Samples were diluted 2-fold in buffer containing 20 mM HEPES pH 7.5, 100 mM NaCl, 1 mM TCEP, 0.02% IGEPAL CA-630, and incubated at room temperature for 10 min. Samples were subjected to chemical crosslinking by addition of a final concentration of 0.2% glutaraldehyde (from a 2.5% stock in water). The samples were incubated at room temperature for 20 min before quenching the crosslinker by addition of 100 mM Tris pH 7.5 (from 1 M stock). To release the crosslinked complexes from the DNA, 10% of the sample volume Pierce universal nuclease, diluted 1:20 in buffer containing 20 mM HEPES pH 7.5, 100 mM NaCl, 5 mM MgCl₂, and 1 mM TCEP, was added. After incubation at room temperature for 10 min, 50 mM EDTA was added to quench the nuclease. Samples were spun down for 15 min at 13 000×g at 4 °C and the supernatant was transferred to a new tube.

Complex formation of CAF-1 and PCNA on linear DNA. Linear DNA fragments with lengths of 18, 33, 43 or 53 bp were mixed with PCNA–C4S–K164C and CAF-1 in buffer containing 20 mM HEPES–KOH pH 7.6, 100 mM KCl, 0.01% IGEPAL CA-630 and 1 mM TCEP, and incubated on ice for 10 min. The final mixture contained 1.5 μ M DNA, 4.5 μ M Alexa Fluor 456 labeled PCNA (concentration for a monomer), and 3 μ M CAF-1. Samples were subjected to chemical crosslinking by diluting 3-fold in the same buffer and addition of a final concentration of 0.2% glutaraldehyde (from a 2.5% stock in water). The samples were incubated at room temperature for 20 min before quenching the crosslinker by addition of 100 mM Tris (from a 25× TAE stock containing 1 M Tris). Samples were spun down for 5 min at 13 000×g at 4°C and the supernatant was transferred to a new tube.

Complex formation of CAF-1–H3–H4 and PCNA without DNA. Histones H3–H4 (C110A,T71C) tetramers, labeled with AlexaFluor 488, were concentrated in 20 mM HEPES pH 7.5, 2 M NaCl, 1 mM EDTA, 1 mM TCEP to a final concentration of 79.4 μ M using an Amicon Ultra-0.5 centrifugal concentrator with a molecular weight cut off of 10 kDa. CAF-1 WT or mutants were diluted to a concentration of 27.1 μ M in 20 mM HEPES pH 7.5, 200 mM NaCl, 1 mM EDTA, 1 mM TCEP. CAF-1 was then mixed with the histones in a volumetric ratio of 3:1 to obtain samples with final concentrations of 20 μ M CAF-1 and 10 μ M H3–H4 tetramers. The NaCl concentration in these samples was around 650 mM. CAF-1–H3–H4 samples were mixed in order with buffer containing 20 mM HEPES pH 7.5, 60 mM NaCl, 1 mM TCEP and then PCNA–C4S–K164C (labeled with AlexaFluor 546, 185 μ M stock) to obtain final concentrations of 1.5 μ M CAF-1–H3–H4, 5.55 μ M PCNA with a total of about 105 mM NaCl. Samples were diluted 2-fold in buffer containing 20 mM HEPES pH 7.5, 100 mM NaCl, 1 mM TCEP, 0.02% IGEPAL CA-630, and incubated at room temperature for 10 min. Samples were subjected to chemical crosslinking by addition of a final concentration of 0.2% glutaraldehyde (from a 2.5% stock in water). The samples were incubated at room temperature for 20 min before quenching the crosslinker by addition of 100 mM Tris pH 7.5 (from 1 M stock). Samples were spun down for 15

min at 13 000×g at 4 °C and the supernatant was transferred to a new tube.

Crosslinking of CAF-1–PCNA on DNA at limiting PCNA concentrations. AlexaFluor546-labeled PCNA K164C (50 nM) was loaded onto nicked (with Nt.BspQ1) pUC19 plasmids (15 nM) by RFC (15 nM). The reaction was conducted at 30 °C for 5 min in buffer containing 20 mM HEPES–KOH pH 7.6, 130 mM NaCl, 0.01% IGEPAL CA-630, 1 mM TCEP, 10 mM MgCl₂, 1 mM ATP. Then, CAF-1 or buffer control was titrated between 0–1 μM. The total NaCl concentration during the loading reaction and after addition of CAF-1, taking into account the contributions from each component, ranged between 100 and 110 mM. After 10 min at room temperature, the samples were diluted 4.5-fold by adding buffer containing 20 mM HEPES–KOH pH 7.6, 100 mM NaCl, 0.01% IGEPAL CA-630, 1 mM TCEP, before cross-linking with 0.2% glutaraldehyde. The cross-linking reaction took place at room temperature for 20 min, after which, it was quenched with a final concentration of 100 mM Tris–HCl pH 7.5. DNA was digested using Pierce™ Universal Nuclease for Cell Lysis (Thermo Fisher Scientific) diluted to 1:20 in 20 mM HEPES–KOH pH 7.6, 100 mM NaCl, 5 mM MgCl₂, 1 mM TCEP and added to 10% of the crosslinking reaction volume. The digestion was quenched with 50 mM EDTA and immediately spun down for 5 min at 13 000×g and 4 °C to remove precipitates.

Crosslinking of FEN1–PCNA at limiting PCNA concentrations. AlexaFluor546-labeled PCNA K164C (50 nM) and FEN1_DA (0–0.6 mM) were mixed in buffer containing 20 mM HEPES–KOH pH 7.6, 100 mM NaCl, 0.01% IGEPAL CA-630, 1 mM TCEP. After 10 min at room temperature, the samples were diluted 4.5-fold by adding buffer containing 20 mM HEPES–KOH pH 7.6, 100 mM NaCl, 0.01% IGEPAL CA-630, 1 mM TCEP, before cross-linking with 0.2% glutaraldehyde. The crosslinking reaction took place at room temperature for 20 min, after which, it was quenched with a final concentration of 100 mM Tris–HCl pH 7.5. Crosslinked samples were immediately spun down for 5 min at 13 000×g and 4 °C to remove precipitates.

SDS-PAGE analysis of crosslinked samples. Crosslinked samples were mixed with 4× XT sample buffer and 20× XT reducing agent in appropriate volumetric ratios (#1610791 and #1610791 from Bio-Rad). These samples were loaded on 12% Criterion XT Bis–Tris gels (#3450118 Bio-Rad) in XT MOPS buffer (#1610793 Bio-Rad). Gels were run at 20 mA until the samples have completely entered the gel and then at 40 mA until the gel run was complete (typically between 2 and 3 h). Gels were run at room temperature, and additionally in the dark if components contained fluorophores. Gels were scanned for histones H3–H4 and/or PCNA fluorescence (depending on the assay) on an AMERSHAM ImageQuant 800 imager (Cytiva). Bands intensity was calculated using the ROI manager tool in Image J/Fiji and plotted using GraphPad Prism. Where applicable, gels were subsequently stained with Coomassie blue and scanned on AMERSHAM ImageQuant 800 imager (Cytiva).

Mass photometry

Samples were prepared using crosslinking at stoichiometric conditions, the reactions (±1.2 ml final volume after EDTA quenching) were concentrated to 500 μl and loaded on a pre-equilibrated Superose 6 10/300 increase GL (Cytiva) column in 20 mM HEPES–NaOH pH 7.5, 200 mM NaCl, 1 mM TCEP. Fractions were analyzed on SDS PAGE, the ones containing the complex of interest (Peak1 or Peak2) were pooled and concentrated to about 40 μl (Abs280 close to 0.5). The samples were diluted 10 to 20-fold in 20 mM HEPES–NaOH pH 7.5, 100 mM NaCl, 1 mM TCEP right before measuring on a Refeyn OneMP instrument (Refeyn Ltd). For each measurement, 13 μl of this buffer was first placed into the CultureWell gaskets wells (Grace Biolabs) placed into the Microscope coverslips (24 mm × 50 mm; Paul Marienfeld GmbH). After adjusting the focus, 2 μl of sample was mixed in. Movies were recorded for 60 seconds at 100 frames per second. A calibration measurement under the same conditions was performed roughly every 15 measurements using an in-house prepared protein standard mixture: IgG4Δhinge-L368A (73 kDa), IgG1-Campath (149 kDa), apoferritin (479 kDa), and GroEL (800 kDa). Data were processed using DiscoverMP (Refeyn Ltd) with bin width adjusted to 10, and each sample retrieved about 1500–3000 counts. Figures were prepared with the Refeyn instrument and edited in Illustrator.

Fluorescence polarization

Fluorescence Polarization assays were carried out in 25 mM TRIS pH 7.5, 300 mM NaCl, 5% glycerol, 1 mM EDTA, 0.01% IGEPAL ca-630 (added fresh), 0.01% CHAPS (added fresh), 1 mM DTT (added fresh). Binding reactions were prepared by mixing 10 nM of Alexa488-labeled H3–H4 (H3 C110A–H4 E63C) and increasing amounts of CAF-1, Pole, Polδ or RPA in a final volume of 30 μl in CORNING low flange 384 well black microplates (CLS3575). Binding data were measured using a CLARIOstar (BMG LabTech) plate reader. The data was analyzed and plotted using Microsoft Excel and GraphPad Prism. *K_d* values were calculated using a one site binding curve in GraphPad Prism. Representative curves are shown from one experiment (three independent measurements) and were repeated at least two times in triplicates.

NAQ assay

This refers to Supplementary Figure S5B. The nucleosome assembly reaction was carried out at 200 nM of 207 bp DNA, 200 nM xenopus octamer maleimide AlexaFluor-647 (AF647) labeled on H2B T112C (containing H3 C110A mutant) and 500 nM CAF-1, Pole or RPA. After the assembly reaction, the samples were diluted to a DNA concentration of 50 nM in 100 μl digestion reactions. 25U of MNase enzyme was added in a final buffer containing 50 mM Tris pH 7.9, 5 mM CaCl₂. After incubation at 37 °C for 10 min, the reactions were quenched with 10 μl of 500 mM EDTA, pH 8. The DNA was then purified using a modified protocol of the MinElute kit from QIAGEN. 550 μl of PB buffer and 10 μl of 3 M sodium acetate were added to each sample and they were incubated at room temperature for 10 min. At this

point, 50 ng of DNA loading control (or reference band, a 621 bp DNA fragment) was added to each tube. The samples were applied to the MinElute spin column and washed as prescribed by QIAGEN. The DNA was eluted with 10 μ l of water. 2.5 μ l were loaded on a 6% PAGE gel. The gel was run for 45 min at 200 V in 0.5 \times TBE buffer at room temperature. Gels were stained with SybrGOLD for DNA and imaged on an AMERSHAM ImageQuant 800 (Cytiva).

Cell culture, genome editing and western blot

Mouse ESCs used in this study were derived from the E14JU cell line with a 129/Ola background. For genome editing and next-generation sequencing experiments, ESCs were grown on gelatin-coated dishes (0.2%) in serum + LIF conditions at 37 °C with 5% CO₂. Media was prepared by supplying DMEM-GlutaMAX-pyruvate with fetal bovine serum (15%), LIF (made in house), 1 \times non-essential amino acids (Gibco), 1 \times penicillin/streptomycin (Gibco) and 2-beta-ME (0.1 μ M). Cells were passaged using Trypsin-EDTA (Gibco) or TrypLE (Gibco). Cells were routinely tested for mycoplasma contamination. For genome editing *Chaf1a*-dTAG cells were generated by CRISPR-Cas9 using the SpCas9(BB)-2A-Puro (PX459) V2.0 plasmid (addgene #62988) as described in (65) with sgRNA#1 (Supplementary Table S5), which target the *Chaf1a* gene at the beginning of the ORF and a *Chaf1*-linker-dTAG homology donor plasmid. Cells were transfected using Lipofectamine 3000 reagent (Invitrogen) using 0.5 μ g of sgRNA-plasmid and 2 μ g of donor plasmid. Cells were sparsely seeded on a 10 cm dish 24 h posttransfection and selected with Puromycin (2 μ g/ml) for 48 h. Thereafter, cells were expanded and genotyped with primers #1 and #2 (Supplementary Table S5). Positive clones were analyzed by Sanger sequencing with primers #3 and #4 (Integrated DNA Technologies, Supplementary Table S5) and degradation upon dTAG-13 (Tocris, 6605) treatment was confirmed by western blot by a-*Chaf1a* antibody (66). Fractionation cell extracts were prepared as in (67). Western blotting was performed as described in (68).

Immunofluorescence

Cells treated with DMSO or dTAG-13 for 4 h, were pulsed in EdU-containing media (10 μ M) for 10 min and immediately fixed for 15 min in 4% PFA at room temperature and stored in PBST (PBS with 0.3% Triton X-100). Primary antibody H4K20me0 was added at the concentration of 1:1000 in PBST with 5% donkey serum and incubated overnight. Incubation was followed by three washes in PBS and secondary antibody was then added in PBST. Samples were incubated with the secondary antibody in the dark at room temperature for 1 h. After three washes, samples were stained with DAPI (1:10 000) in PBST. Images were acquired with a ScanR high-content screening microscope (Olympus). Automated and unbiased image analysis was carried out with the ScanR analysis software (version 2.8.1). Individual cells were identified based on DAPI staining and mean pixel intensity was measured for each channel. Data were exported and processed using Spotfire software (version 10.5.0; Tibco). Statistical analysis and visual-

ization of results was done using using R (v4.1.2) in RStudio (v2021.9.2.382).

SCAR-seq

A step-by-step protocol is available (69). Briefly, nascent SCAR-seq samples were prepared from *Chaf1a*-dTAG cells in three biological replicates for each histone PTM. Cells treated with DMSO or dTAG-13 for 2 h, were pulsed in EdU-containing media (10 μ M) for 30 min and harvested immediately. For sample collection, media was aspirated, plates washed 2 \times with room temperature PBS and ice-cold PBS was added to the dishes. Cells were scraped in a cold room and collected by centrifugation, followed by nuclei isolation. Nuclei were aliquoted, snap-frozen and stored at -80°C until further use. For MNase digest, nuclei were counted manually using Kova Glasstic Slides and 2 U MNase (Worthington) were added per 1 \times 10⁶ nuclei. Digests were performed at 30°C for 20 min. For native ChIP, 30–50 μ g of chromatin was used per sample and incubated with antibodies in a total volume of 600 μ l overnight at 4°C with H3K27me3 antibody (Cell Signaling, 9733) or H4K20me0 antibody (Abcam, ab227804). Magnetic beads (anti-rabbit IgG Dynabeads, invitrogen) were added the next morning and samples were incubated for 2 h. After three washes each with ice-cold RIPA buffer and RIPA 0.5M NaCl buffer, DNA was eluted and purified using the MinElute Reaction Cleanup kit (Qiagen). Mononucleosomal-sized fragments were isolated by double sided size selection with AMPure XP beads (Beckman Coulter). EdU-labelled DNA fragments were biotinylated using Click-iT chemistry as reported above but using Biotin-TEG-Azide (Berry & Associates) instead of Picolyl-azide-PEG4-Biotin. Libraries were prepared using the KAPA Hyper Prep Kit (Roche). Biotinylated fragments were captured using Dynabeads MyOne Streptavidin (invitrogen) and EdU strands were purified by performing NaOH washes. Libraries were amplified in 9–11 PCR cycles. Libraries with mononucleosomal-sized inserts were isolated by double-sided size selection with AMPure XP beads (Beckman Coulter), followed by a second clean-up with 1.0 \times AMPure XP beads. Fragment distribution of libraries was checked on a Fragment Analyzer system (Agilent). Stranded input samples were prepared in parallel with SCAR-seq samples. Samples were sequenced single end (75bp) on a NextSeq500 instrument (Illumina).

Reads were processed, mapped and histone partition signal was computed as described previously (68). Briefly, for each strand the SCAR normalized signal (CPM) was computed in 1kb bins and smoothed in a uniform blur considering the neighbouring 30 bins on each side. For each 1kb window, the signal from its corresponding SCAR input was subtracted and negative values were set to zero. Input corrected windows with CPM 0.3 on both strands were filtered out and not considered for further analyses. The final partition score for each 1kb window was calculated as: partition = (F – R)/(F + R) where F and R correspond to the number of normalized and input-corrected reads for the forward and reverse strand, respectively. The partition value relates to the ratio of histones with a specific modification being segregated to the nascent forward (par-

tition > 0) or nascent reverse (partition < 0) strand within each window respectively. Okazaki-seq replication fork directionality (RFD) scores and filtered initiation zones (IZs) for mESC were taken from (68) and used to define replication via leading or lagging strand mechanism. The RFD score in Okazaki-seq is calculated like SCAR-seq partition scores but subtracting the forward (F) strand signal from the reverse (R) strand signal instead: $RFD = (R - F)/(F + R)$.

The average partition signal from replicate 1 was used for visualization purposes in Partition line plots (Figure 6). To visualize the total reads in SCAR-seq, total mm10 mouse read counts were spike-in normalized to dm6 drosophila read counts as described in (70) By using the uniquely mapping, deduplicated reads in millions, the EdU-enriched Input samples ('ClickedInputs') was used as reference for relative spike-in abundance and EdU labelling efficiency. To visualize global signal in SCAR-seq, number of uniquely mapped, deduplicated mm10 reads of the SCAR sample (in million reads) were normalized to DMSO for each mark and replicate and plotted in replicates using R (v4.1.2) in RStudio (v2021.9.2.382).

End-point DNA replication with yeast replisome

These were carried out as in (9), all stock protein concentrations were determined by Bradford analysis. MCM was loaded onto 5.8 Kb ARS1 plasmid in 30 μ l reaction volumes, to final concentrations of 22.5 nM ORC, 100 nM Mcm2/7-cdt1, 45 nM Cdc6 and 4 nM plasmid DNA template, in buffer containing 25 mM HEPES-KOH pH 7.6, 100 mM potassium glutamate, 10 mM magnesium acetate, 0.02% IGEPAL CA-630, 5% glycerol, 5 mM ATP, 0.1 mg/ml BSA, 1 mM DTT. This reaction was incubated at 30°C for 20 min. After origin licensing, DDK was added to 25 nM and further incubated at 30°C for 30 min. The replication reaction was initiated by addition of FF500 buffer (50 mM HEPES-KOH pH 7.6, 500 mM potassium glutamate, 20 mM magnesium acetate, 0.02% IGEPAL CA-630, 2 mM DTT, 6 mM ATP, 0.2 mg/ml BSA, 0.4 mM CTP, GTP, UTP each, 0.16 mM dGTP, dATP, dTTP, dCTP and 40 nM α 32P-dCTP), followed by replication proteins in a master mix added to final reaction concentrations of 30 nM Dpb11, 40 nM cdc45, 210 nM GINS, 20 nM S-CDK, 5 nM Mcm10, 25 nM Sld3/7, 50 nM Sld2, 20 nM Pole, 100 nM RPA, 20 nM Pol α , 20 nM Ctf4, 20 nM TopoII, and another protein master mix added to final reaction concentrations of 20 nM Mrc1, 20 nM Csm3/Tof1, 10 nM TopoI, 20 nM RFC, 20 nM PCNA, 10 nM Pol δ . The replication reaction was conducted at 30 °C for 40 min. After this, the reaction was quenched by addition of 50 mM EDTA to 2 \times dilution. Samples were cleaned-up for unincorporated nucleotides using MicroSpin G-50 columns (Cytiva), after which they were denatured in 100 mM NaOH, 2% sucrose, bromocresol green as loading dye and 15 μ l samples were run on 0.7% alkaline agarose gels for 18 h at 45 V. The next day, DNA was precipitated on gel by treatment with ice cold 5% TCA for 2 cycles of 15 min with TCA refreshment. The gel was dried in 2 \times chromatography Whatman paper and towel paper sandwich with a weight on top for 30 min, to remove excess moisture. After that, the Whatman paper gel

sandwich was moved to a gel dryer for 2.5 h at 55°C. Gel was exposed to a phosphor screen for 2 days using Amersham Typhoon Biomolecular Image.

Pulse-chase experiments

These were carried out as in (9), all stock protein concentrations were determined by Bradford analysis. MCM was loaded onto 5.8 Kb ARS1 plasmid in 150–300 μ l reaction volumes, to final concentrations of 22.5 nM ORC, 100 nM Mcm2/7-cdt1, 45 nM Cdc6 and 4 nM plasmid DNA template, in buffer containing 25 mM HEPES-KOH pH 7.6, 100 mM potassium glutamate, 10 mM magnesium acetate, 0.01% IGEPAL CA-630, 5 mM ATP, 0.1 mg/ml BSA, 1 mM DTT. This reaction was incubated at 30°C for 30 min. After origin licensing, DDK was added to 25 nM and further incubated at 30°C for 30 min. Replication proteins in a master mix were added to final pulse reaction concentrations of 30 nM Dpb11, 40 nM cdc45, 210 nM GINS, 20 nM S-CDK, 5 nM Mcm10, 25 nM Sld3/7, 50 nM Sld2, 20 nM Pole, 100 nM RPA, 40 nM Pol α , 20 nM Ctf4, followed by another protein master mix added to final pulse reaction concentrations of 20 nM Mrc1, 20 nM Csm3/Tof1, 10 nM TopoI. This reaction was then split into the pulse mixes containing 20 nM RFC, 20 nM PCNA, 180 nM CAF-1 or FEN1 (or corresponding storage buffers for control reactions), FF500 pulse buffer (50 mM HEPES-KOH pH 7.6, 500 mM potassium glutamate, 20 mM magnesium acetate, 0.02% IGEPAL CA-630, 2 mM DTT, 6 mM ATP, 0.2 mg/ml BSA, 0.4 mM CTP, GTP, UTP each, 0.16 mM dGTP, dATP, dTTP, 4 μ M dCTP and 66 nM α 32P-dCTP. Pulse reaction was conducted at 30 °C for 3 min 20 sec, when the chase (0.6 mM dCTP, dGTP, dATP, dTTP) was added. Time points were taken (15 μ l) at 4, 5, 6 and 7 min and replication reaction was quenched by addition to 2 \times dilution in 50 mM EDTA. Samples were cleaned-up for unincorporated nucleotides using MicroSpin G-50 columns (Cytiva), after which they were denatured in 10 mM NaOH, 2% sucrose, bromocresol green as loading dye and 14 μ l samples were run on 0.7% alkaline agarose gels for 18 h at 45 V. The next day, DNA was precipitated on gel by treatment with ice cold 5% TCA for 2 cycles of 15 min with TCA refreshment. The gel was dried in 2 \times chromatography Whatman paper and towel paper sandwich with a weight on top for 30 min, to remove excess moisture. After that, the Whatman paper gel sandwich was moved to a gel dryer for 2.5 h at 55 °C. Gel was exposed to a phosphor screen for 2 days using Amersham Typhoon Biomolecular Image.

Max replication rate quantification

Data analysis was performed using the ImageQuant TL software. The raw data was analyzed using the 1D gel analysis option. Lanes were created manually with a 95% lane width. The background subtraction was done automatically using the minimum profile option. The peak of leading strand signal was selected manually under band detection in each lane. The upper boundary of the leading strand products, i.e. the front of the peak (created automatically by ImageQuant), was used as the max size of replicated products (example is shown in Supplementary Figure S7C). To con-

vert mm to bp, a lane was created for the marker. The molecular size calibration was done using the standard ladder product sizes of Lambda DNA digested with HindIII. The conversion was computed automatically within the software using a log curve and Retardation factor (Rf) to propagate the values. The bp values calculated by ImageQuant for the earliest three time-points after addition of the chase were used in in GraphPad prism to fit a linear regression, whose slope determined the max replication rates reported. To compare these rates independently on the variability of replication speed between experiments, we also normalized within each repeat the max replication rate of all conditions to the one of the + RFC/PCNA (no CAF-1) sample.

RESULTS

CAF-1 recruitment to PCNA requires DNA

We first set out to study the interaction between CAF-1 and PCNA in the context of DNA, as this is the context in which the CAF-1–PCNA interaction occurs during DNA replication. Therefore, we loaded PCNA onto nicked plasmids using the ATP-dependent clamp loader RFC1-5 (71), and separated DNA-loaded from free PCNA on a size exclusion column (SEC) (Supplementary Figure S1A) (72). When adding CAF-1, we observed that the three CAF-1 subunits co-eluted with DNA-loaded PCNA, suggesting the formation of a CAF-1–PCNA–plasmid complex (Figure 1A and Supplementary Figure S1B, C). As CAF-1 uses PIPs to bind PCNA in cells (38,51–53), we introduced mutations in these domains to test their importance in our *in vitro* system (Supplementary Figure S1D). The mutant CAF-1_PIP** no longer bound to DNA-loaded PCNA (Figure 1B and Supplementary Figure S1C), confirming that our *in vitro* reconstitution recapitulates the physiological determinants of the CAF-1–PCNA interaction.

Next, we investigated how DNA contributes to the CAF-1–PCNA interaction. CAF-1 did not co-elute with PCNA in the absence of DNA (Supplementary Figure S1E) or when PCNA was not loaded onto DNA (i.e. by omission of ATP) (Figure 1C and Supplementary Figure S1C), suggesting that DNA is required for the CAF-1–PCNA interaction. To confirm that the interaction between CAF-1 and PCNA is DNA-dependent, we crosslinked CAF-1 to fluorescently labeled PCNA on nicked DNA plasmids using glutaraldehyde, followed by nuclease digestion and SDS-PAGE analysis to determine if more transient protein–protein complexes are formed in solution, which may be lost during the SEC purification. Again, we observed significant CAF-1–PCNA complexes only when PCNA was loaded onto DNA (Figure 1D). These results indicate that DNA is required for a stable interaction between CAF-1 and PCNA.

CAF-1 contains two DNA binding regions in its large Cdc1 subunit: the Lys–Glu–Arg rich (or KER) region located at the N-terminus, which is flanked by the PIPs, and the winged-helix domain (WHD) at the C-terminus (Supplementary Figure S1D). Either domain is required for CAF-1 function in cells (46,52,73–74), but their relative role in CAF-1 mechanism remains unclear, as both domains must be mutated simultaneously in order to disrupt CAF-1 activity *in vitro* in the absence of PCNA (54). We

thus tested whether these domains contributed to the DNA-dependent interaction of CAF-1 to PCNA. Deletion of the KER domain or its mutation into a neutral unstructured sequence (CAF-1_ΔKER and CAF-1_KER*, respectively) abrogated the interaction between CAF-1 and DNA-loaded PCNA, similarly to the effect of the CAF-1_PIP** mutant (Figure 1E and Supplementary Figure S1F). However, mutations in the WHD (CAF-1_WHD*) had no effect on binding to DNA-loaded PCNA (Figure 1F). These results indicate that the CAF-1 KER domain, but not the WHD, is critical for the formation of a stable CAF-1–PCNA complex on DNA.

Having established that DNA is required for the CAF-1–PCNA interaction, we investigated whether there is a minimum DNA length required to promote this interaction. We first confirm that CAF-1 binds 10-fold more weakly to a 18 bp DNA ($K_d > 2 \mu\text{M}$) than to a 33, 43 or 53 bp DNA ($K_d = 0.33, 0.23$ and $0.18 \mu\text{M}$ respectively) (Supplementary Figure S1G), in line with previous observations (75). Mutations in the KER domain strongly inhibit the CAF-1–DNA interaction, while WHD mutations have a minor effect (Supplementary Figure S1H). Complex formation was less efficient on the 18 bp DNA fragment, where PCNA can load in the absence of RFC, than on the longer 43 and 53 bp DNAs (Figure 1G and Supplementary Figure S1I). This suggests that a minimum of ± 30 bp need to be exposed for CAF-1 to stably bind PCNA on DNA. Notably, the AlphaFold model of the Cdc1-KER domain (residues 128–226) predicts a long helical structure of $\sim 145 \text{ \AA}$, which is confirmed by a very recent crystal structure (76) and corresponds to the length of ~ 44 bp of duplex DNA (Supplementary Figure S1J). This domain displays a positively charged surface along its helical arrangement, which may structurally explain the link we observe between DNA length and CAF-1 binding, assuming that this surface interacts with the negatively charged phosphate backbone of the DNA via electrostatic interactions. Overall, these observations suggest that the CAF-1–PCNA interaction on DNA is stabilized by DNA of at least ~ 30 bp via the KER domain in CAF-1.

Reconstitution of PCNA-dependent nucleosome assembly by CAF-1

In cells, PCNA directs CAF-1 mediated chromatin assembly (42,48–49,51). However, we and others have recently shown that CAF-1 is able to assemble nucleosomes *in vitro* in the absence of other factors (54,75,77). To determine how the presence of PCNA affects the histone chaperone activity of CAF-1, we set out to develop a nucleosome assembly assay that recapitulates the PCNA dependency of CAF-1 activity observed *in vivo*. The challenge is to differentiate between PCNA-dependent and PCNA-independent (i.e. purely DNA driven (54)) activity of CAF-1. To overcome this challenge, we mixed a nicked plasmid where PCNA can be loaded, with a competitor negatively supercoiled plasmid where PCNA-independent CAF-1 activity takes place efficiently. Following a PCNA loading step, we added CAF-1–H3–H4 complexes to promote tetramer deposition followed by the addition of fluorescently labeled H2A–H2B, which associate with tetrasomes *in vitro* to form nucleosomes. To measure PCNA-dependent nucleosome assembly, we quan-

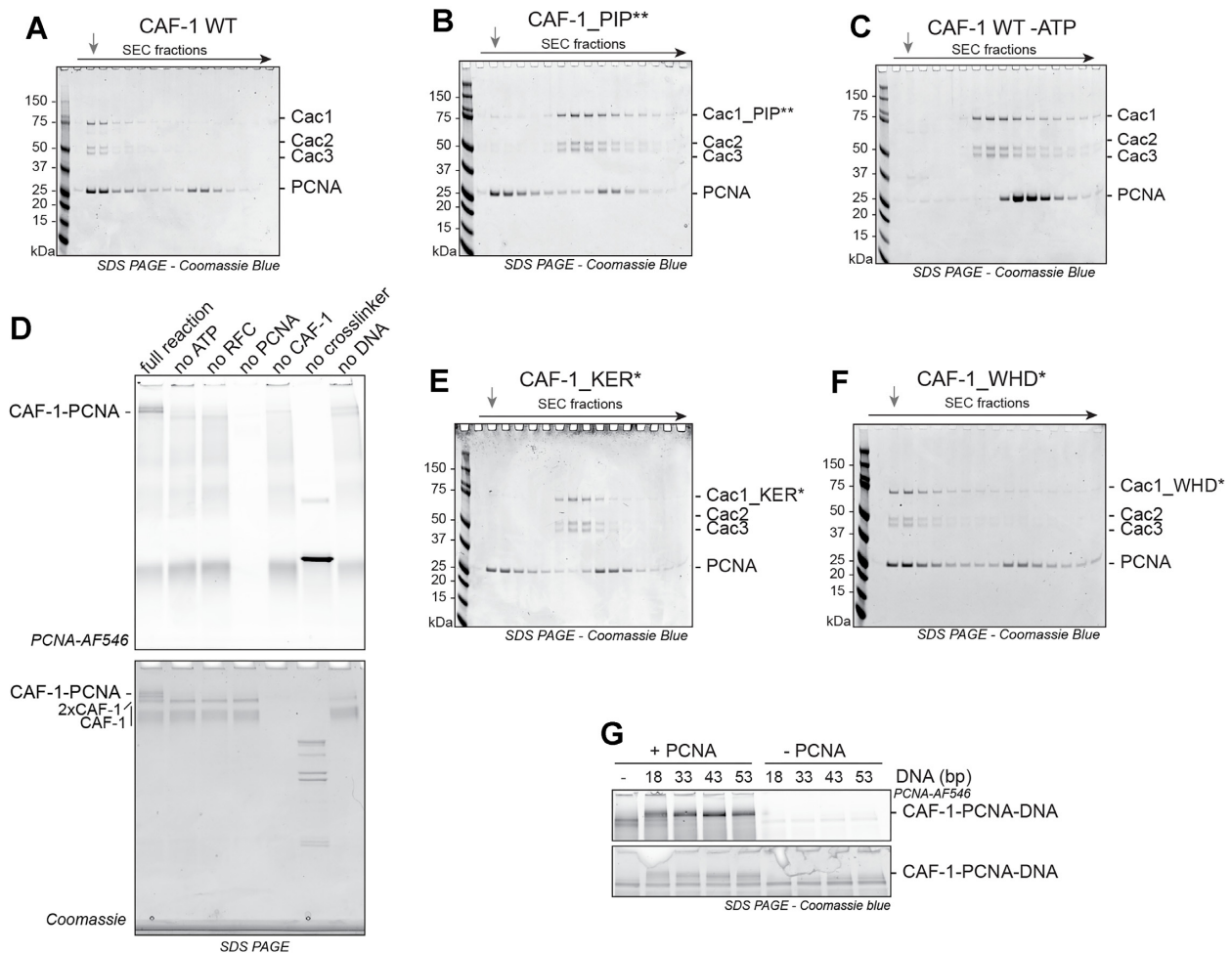


Figure 1. DNA controls CAF-1 recruitment to DNA-loaded PCNA. (A–C) SDS PAGE following separation on SEC of a CAF-1–PCNA binding reaction on DNA plasmids using WT CAF-1 (A), a CAF-1_PIP** mutant (B), or WT CAF-1 in absence of ATP (C). The grey arrow indicates the elution volume of the plasmid DNA. Chromatograms are shown in Supplementary Figure S1C. (D) SDS PAGE of glutaraldehyde crosslinking reactions of fluorescent PCNA (3 μM), CAF-1 (1.5 μM), RFC (150 nM) and nicked pUC19 plasmid (300 nM) after nuclease digestion. Fluorescence scan for PCNA (546 nm) and Coomassie staining are shown. The CAF-1 and PCNA interaction is dependent on PCNA loading onto DNA. (E, F) Coomassie-stained SDS PAGE following SEC of a CAF-1–PCNA binding reaction on DNA plasmids using CAF-1_KER* (E) and CAF-1_WHD* (F) mutants. (G) Crosslinking experiment between CAF-1 (3 μM) and labeled PCNA (4.5 μM) on DNA fragments (1.5 μM) of various sizes. RFC and ATP were not added to actively load PCNA and DNA was not digested in these reactions. Full gels are shown in Supplementary Figure S11.

tify the histones fluorescence signal on the nicked plasmid relative to the total histone signal on both plasmids in each lane. Micrococcal nuclease (MNase)-based analysis of nucleosome fragments (± 150 bp) are also used to assess nucleosome formation. We named this setup PCNA-NAQ assay, based on our previously established Nucleosome Assembly and Quantitation (NAQ) assay (54,63).

We first established that the PCNA-NAQ assay measures PCNA-dependent and -independent CAF-1 activity. Efficient nucleosome assembly (monitored by an increase in H2B fluorescence) on the nicked plasmid was observed only when PCNA is loaded on DNA and CAF-1 is present (Figure 2A). When PCNA loading was blocked by the omission of ATP, PCNA or RFC (Figure 2A), the histone fluorescence signal shifted to the supercoiled plasmid, confirming that the signal on the nicked plasmid is largely dependent on PCNA. As expected, omission of CAF-1 led to a drastic reduction of histone deposition (Figure 2A and Supple-

mentary Figure S2A), reinforcing that CAF-1 is the nucleosome assembly machinery on both plasmids in our reconstitution. No nucleosomes were formed upon omission of either histones H3–H4 or H2A–H2B (Supplementary Figure S2B). Moreover, using labeled H3–H4 instead of H2A–H2B did not affect these results (Supplementary Figure S2C), confirming that our signal is a *bona fide* measure of assembled nucleosomes. Quantification of the histone fluorescence signal on the nicked plasmid compared to total histone signal showed that roughly 50% of the nucleosomes are assembled in a PCNA-dependent manner, when PCNA is loaded (Figure 2B). This is reduced to roughly 20% when PCNA was not loaded onto DNA (Figure 2B). These observations were confirmed using next generation sequencing approaches of the MNase products, when we used plasmids with distinct DNA sequences which allowed us to map relative nucleosome assembly and positioning (Supplementary Figure S2D–G). Thus, we developed a new method

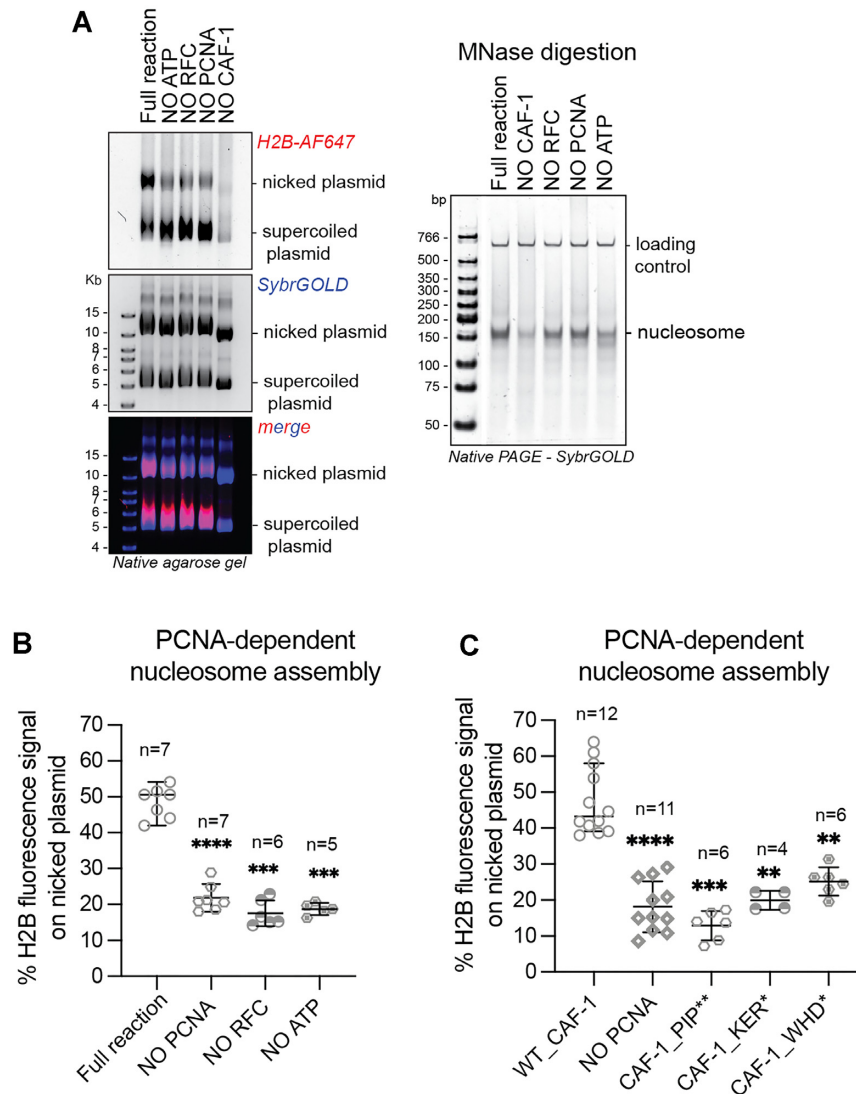


Figure 2. The WHD of CAF-1 controls PCNA-dependent nucleosome assembly. (A) (Left) Native agarose gel of PCNA-NAQ assay reactions. A reaction containing all components, and reactions where we removed either ATP, RFC, PCNA or CAF-1 are shown. Fluorescence signal for H2B-T112C labeled with AF647 (H2B-AF647) or DNA (SybrGOLD), and their overlay are shown. H2B fluorescence on the nicked plasmid (top panel) represents PCNA-dependent histone deposition. (Right) Native PAGE stained with SybrGOLD to detect protected DNA fragments following MNase digestion of samples in A. 150bp DNA fragments are characteristic of nucleosomal DNA, a 621bp loading control is used to monitor DNA retrieval during the purification procedure. Bands around 120bp represent hexasomes. (B) Quantification of the H2B fluorescence signal on the nicked plasmid relative to the total H2B signal in each lane in panel A as a measure of PCNA-dependent nucleosome assembly. (C) Quantification of the PCNA-dependent nucleosome assembly activity for CAF-1_PIP**, CAF-1 KER* and CAF-1_WHD*. Mean \pm SD is shown, * $P < 0.05$, ** $P < 0.01$, *** $P < 0.001$, **** $P < 0.0001$ (one-way ANOVA comparing WT CAF-1 to control conditions (B) or each mutant (C)). Gels are shown in Supplementary Figure S2H.

to study the PCNA-dependent nucleosome assembly function of CAF-1, where we can distinguish and quantify the PCNA-dependent or PCNA-independent activities of this histone chaperone complex.

We then used this method to understand how CAF-1 assembles nucleosomes when bound to PCNA. We first tested if mutations in the KER domain or PIPs of Cac1, which are important for recruitment to DNA-loaded PCNA (Figure 1B, E), affected its PCNA-mediated activity. As expected, CAF-1_KER* and CAF-1_PIP** showed a reduction specifically in PCNA-dependent nucleosome assembly (Figure 2C and Supplementary Figure S2H), while the overall activity of the mutant complexes was not affected as

seen by the consistent level of MNase-protected nucleosome fragments (Supplementary Figure S2H). This confirms that CAF-1 recruitment is necessary for PCNA-dependent nucleosome formation in our PCNA-NAQ assay, further validating the role of these domains in the CAF-1-PCNA interaction. Strikingly, the CAF-1_WHD* mutant also showed a decrease in PCNA-dependent nucleosome assembly activity (Figure 2C and Supplementary Figure S2H), despite being able to bind DNA-loaded PCNA (Figure 1F) and being fully active in nucleosome assembly in absence of PCNA as shown by the MNase digestion products (Supplementary Figure S2H). This demonstrates that the WHD domain is important for PCNA-dependent CAF-1 activity speci-

cally. Our observations explain why WHD mutations affect chromatin assembly during DNA replication in yeast cells (52,54,74), and why previous *in vitro* reconstitutions that omitted PCNA were unable to recapitulate loss of function of this mutant (54,75). In summary, we show that the WHD domain in CAF-1 is important for the PCNA-dependent nucleosome assembly function of the complex.

Two CAF-1 complexes bind PCNA to assemble nucleosomes

Two CAF-1 complexes are required to assemble one nucleosome in the absence of PCNA (54,75). To understand how CAF-1 assembles nucleosomes when bound to PCNA, we therefore set out to study the stoichiometry of the CAF-1–PCNA complex on DNA. To this end, we used protein-protein crosslinking followed by nuclease digestion and SEC to analyze complexes in solution. These reaction products elute in two peaks of equal distribution (Figure 3A). We collected fractions from these peaks and analyzed them by mass photometry to determine their composition (78). We found that Peak1 (Figure 3A) contained CAF-1–PCNA complexes corresponding to predominantly two CAF-1 per PCNA trimer (~430 kDa), and a lower amount of three CAF-1 per PCNA trimer (~590 kDa) (Figure 3B), while Peak2 contained mostly free unbound CAF-1 (~190 kDa) and a small fraction of complexes containing one CAF-1 per PCNA trimer (~285 kDa) (Figure 3B). In line with RFC being present at substoichiometric concentrations in these samples, no RFC-containing complexes are detected in these experiments (RFC Δ N weights 220 kDa). These data indicate that the CAF-1–PCNA complex mainly assembles in a 2:1 (CAF-1 to PCNA trimer) stoichiometry on DNA, and to a lesser extent can form 3:1 or 1:1 assemblies.

To further evaluate the stoichiometry of CAF-1–PCNA–DNA complexes, we monitored complex formation using crosslinking at limiting concentrations of fluorescently labeled PCNA loaded onto DNA, which also allows us to estimate binding affinities. Without CAF-1, PCNA crosslinks with the clamp loader RFC. On gel, this complex runs at the same height as the 2 \times CAF-1–PCNA complex (Figure 3C and Supplementary Figure S3A). As we titrate CAF-1 above 100 nM, while maintaining RFC constant at 15 nM, this band increases in intensity (Figure 3C, D and Supplementary Figure S3A), indicating the formation of the CAF-1–PCNA complex. Interestingly, above 350 nM, we observed that 3 \times CAF-1–PCNA complexes formed while the 2 \times CAF-1–PCNA band became less pronounced (Figure 3C, D and Supplementary Figure S3A). We observed only a small fraction of 1 \times CAF-1–PCNA complexes (Figure 3C–D and Supplementary Figure S3A) in line with the mass photometry results (Figure 3B). Together, these experiments demonstrate that CAF-1 prefers to bind PCNA on DNA with a 2:1 stoichiometry at concentrations around 100 nM. Above 350 nM, additional CAF-1 complexes can associate with DNA-loaded PCNA. Interestingly, only a very small fraction of CAF-1–PCNA complexes at a 1:1 stoichiometry is observed. This is in line with our previous observation that two CAF-1 complexes cooperatively associate on DNA (54,75), and it shows that it also applies to PCNA-dependent CAF-1 chromatin assembly.

To ask if this assembly is important for CAF-1 histone chaperone function, we tested if mutations in the WHD domain affected the stoichiometry of CAF-1–PCNA complexes. Indeed, the WHD is important for the cooperative DNA binding of CAF-1 and for its function in cells (54), and mutations in the WHD affect the PCNA-dependent nucleosome assembly activity of CAF-1 in the PCNA-NAQ assay (Figure 2C). CAF-1.WHD* affected the composition of CAF-1–PCNA complexes, with a reduction in the formation of 2:1 or 3:1 CAF-1–PCNA complexes in solution (Figure 3E). This explains why this complex is inactive in PCNA-dependent nucleosome assembly (Figure 2C) and argues that two CAF-1 complexes are required for histone deposition also in the context of PCNA.

Histones further promote the CAF-1–PCNA interaction

Although histones are not strictly required for the formation of a CAF-1–PCNA complex on DNA (Figure 1), CAF-1 tightly binds H3–H4 during DNA replication. Thus, we set out to investigate if histones affect CAF-1 binding to PCNA. To this end, we investigated the role of histones on the CAF-1–PCNA interaction in the absence of DNA, because in DNA-containing reactions histones would be immediately deposited onto DNA, making it impossible to assess their effect on the CAF-1–PCNA interaction. As shown above, CAF-1 does not bind to PCNA when DNA is missing from the reaction (Supplementary Figure S1E). However, pre-incubation of CAF-1 with H3–H4 promotes the interaction between CAF-1 and PCNA in the absence of DNA in crosslinking experiments (Figure 3F). Deletion of the N-terminal region in Cdc1, which contains the PIPs and KER domain (as in the truncated tCAF-1 construct, Supplementary Figure S1D), prevents the CAF-1–PCNA interaction (Figure 3F), confirming that this region is responsible for binding to PCNA within the complex. Interestingly, the interactions between CAF-1–H3–H4 and PCNA in the absence of DNA could not be observed from a SEC purification (Supplementary Figure S3B), suggesting that it is more dynamic than the interaction that is mediated by DNA.

Previous work has shown that H3–H4 binding to the CAF-1 acidic domain induces conformational changes at the PIPs, KER and WHD regions, that are important for CAF-1 histone chaperone function (54,77). These conformational changes could be mimicked by deleting the acidic domain in CAF-1 (54), we thus generated a mutant carrying such deletion (CAF-1 Δ AD) to test if these conformational changes control the CAF-1–PCNA interaction. Strikingly, crosslinking between full-length CAF-1 Δ AD and PCNA shows efficient complex formation in absence of DNA and histones in crosslinking experiments (Figure 3G). Moreover, CAF-1 Δ AD efficiently forms complexes with PCNA on DNA at lower concentrations than WT CAF-1 (below 100 nM, Supplementary Figure S3C), suggesting an increase in binding affinity for this mutant to DNA-loaded PCNA. These data argue that changes that occur upon neutralization of the acidic domain (i.e. mimicking histone binding) in CAF-1 promote interactions with PCNA. Together these data suggest that histones are not required *per se* for PCNA binding on DNA, however they

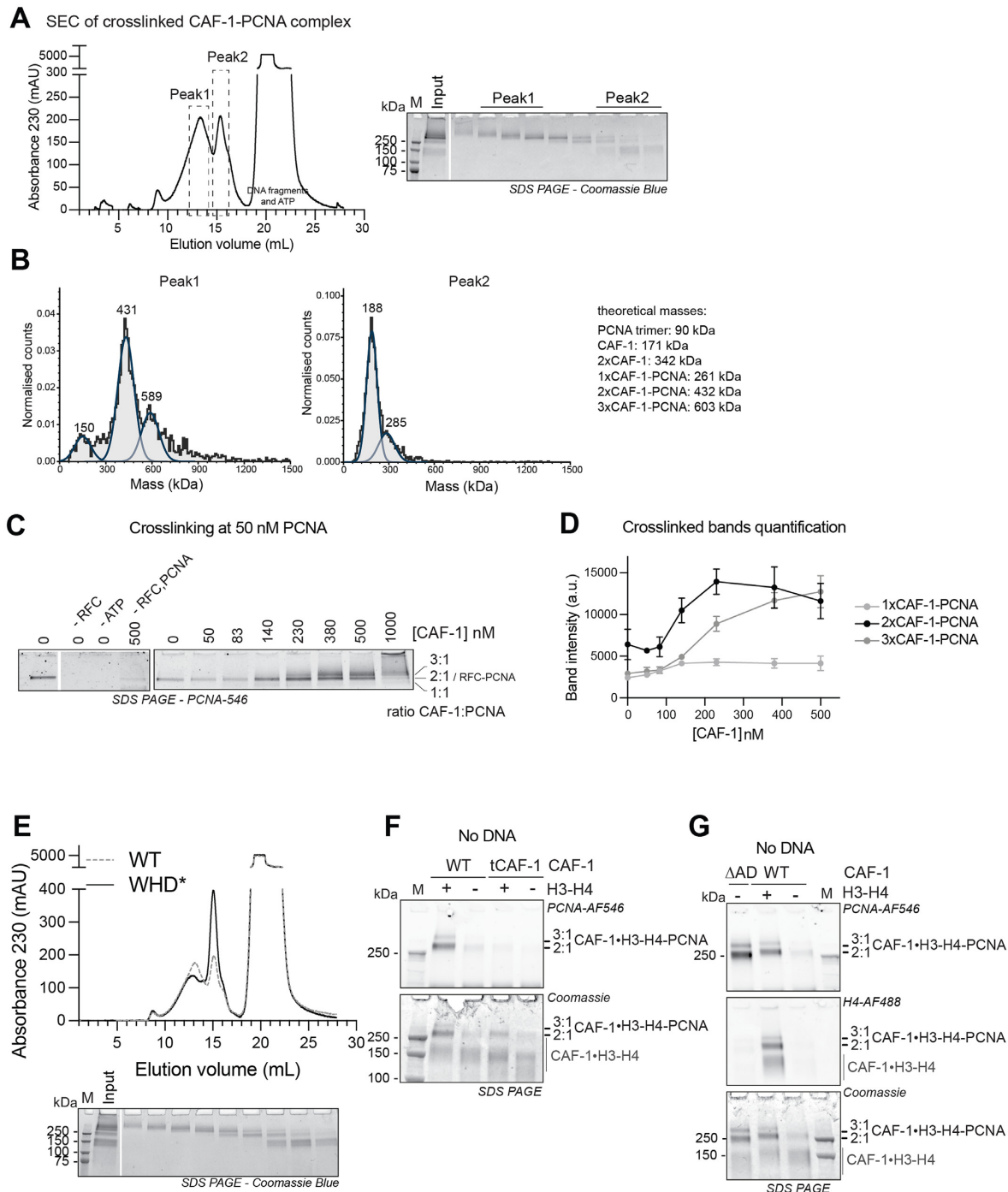


Figure 3. Two CAF-1 complexes bind to DNA-loaded PCNA and histones regulate this interaction. (A) (Left) SEC of crosslinked CAF-1-PCNA complexes after DNA digestion using 1 μ M PCNA, 0.15 μ M RFC, 1.5 μ M WT CAF-1 and 0.3 μ M nicked pUC19. After crosslinking with 0.2% glutaraldehyde and quenching, the samples were treated with nuclease to digest the DNA plasmid. (Right) Coomassie SDS-PAGE of the collected fractions. The fractions that were used to prepare mass photometry samples are shown as Peak1 and Peak2. (B) Mass photometry data of pooled fractions of Peak1 (left) and Peak2 (right) from experiment in panel A. Theoretical masses are listed and calculated masses from the fitted data are shown in each graph. Normalized counts are shown. (C) SDS PAGE of protein-protein crosslinking reactions after DNA digestion. These reactions contain 50 nM fluorescently labeled PCNA, 15 nM full-length RFC, 15 nM pUC19 and increasing CAF-1 concentrations. PCNA fluorescence signal is shown. Full gels are shown in Supplementary Figure S3A. (D) Quantification of the fluorescence intensity of bands in C. Data are shown as mean \pm SD of three independent experiments. (E) SEC and SDS-PAGE of crosslinked CAF-1-PCNA complexes after DNA digestion with CAF-1-WHD*, as in panel A. WT curve is shown in dashed gray line for comparison. (F) SDS PAGE of crosslinking reactions containing fluorescent PCNA (5.5 μ M) and H3-H4 (H4-E63C, 1.5 μ M dimer concentration), CAF-1 or tCAF-1 (1.5 μ M). DNA or RFC are not present in these reactions. (G) SDS PAGE of crosslinking reactions containing fluorescent PCNA (5.5 μ M) and H3-H4 (H4-E63C, 1.5 μ M dimer concentration), CAF-1 or CAF-1- Δ AD (1.5 μ M). DNA or RFC are not present in these reactions.

may promote the CAF-1–PCNA interaction via conformational changes that involve the N-terminal region in Cca1.

CAF-1 inhibits DNA synthesis by Pole, but not Pol δ , via PCNA

At replication forks PCNA binds several proteins, most prominently the replicative DNA polymerases on both daughter strands. As replicated DNA is readily assembled into chromatin at replication forks (21,22), we next asked how DNA polymerases and CAF-1 may share or compete for binding to PCNA.

To this end, we first investigated the effects of CAF-1 on PCNA-mediated DNA synthesis by the leading- and lagging-strand DNA polymerases Pole and Pol δ , in a primer extension assay. In this assay, the extension of a fluorescent DNA primer that is annealed to an RPA-coated single stranded plasmid is monitored over time. As previously shown, yeast Pol δ and Pole efficiently synthesized DNA in a PCNA-dependent fashion with distinct kinetics (Supplementary Figure S4A) (15–17,79). We found that adding CAF-1 had minimal effects on DNA synthesis by Pol δ in this primer extension assay (Figure 4A). However, CAF-1 had a strong inhibitory effect on DNA synthesis by Pole, at concentrations of 150 nM where CAF-1 may bind PCNA with a 2:1 stoichiometry (Figures 4B, 3D). This effect was dose-dependent and indicative of competitive inhibition (Figure 4B and Supplementary Figure S4B). This suggests a dynamic and steric effect of CAF-1 on Pole-mediated DNA synthesis, and not on Pol δ . To test if the inhibition of Pole involved a crosstalk on PCNA, we used CAF-1 mutants that do not bind to DNA-loaded PCNA (i.e. CAF-1_PIP** and CAF-1_KER*). These mutants did not inhibit Pole activity (Figure 4C–D), demonstrating that the inhibitory effect of CAF-1 on Pole is exerted via PCNA. These data are consistent with CAF-1 and Pole competing for binding on PCNA.

Previous studies have shown that Pol δ has a higher binding affinity for PCNA ($K_{d,app} = 13.7$ nM) than Pole ($K_{d,app} = 326$ nM) (17). We found that CAF-1 binds PCNA on DNA with intermediate binding affinity (~100 nM) (Figure 3C, D). Therefore, we tested whether Pol δ might simply outcompete CAF-1 on PCNA, unlike Pole. To this end, we first used the CAF-1_ Δ AD mutant which shows tighter binding to DNA-loaded PCNA (estimated $K_d < 50$ nM, in the same range as Pol δ) (Supplementary Figure S3C). While inhibiting Pole even more strongly than WT CAF-1, this mutant had a minor effect on Pol δ activity when added at 300 nM (Supplementary Figure S4C). This suggests that interactions of CAF-1 with PCNA are possible during Pol δ -dependent synthesis, and Pol δ is largely unaffected by these CAF-1 interactions. In addition, we wanted to test if other PIP-containing proteins that bind PCNA with similar affinities could phenocopy the CAF-1 effects on the two polymerases. To this end, we used a catalytic-dead version of *Xenopus laevis* FEN1 D181A (FEN1_DA), which binds yeast PCNA as a monomer in a PIP-dependent manner and with affinities that are comparable to CAF-1 (Supplementary Figure S4D) (80). FEN1 did not inhibit Pol δ (81) or Pole in primer extension experiments (Figure 4E, F and Supplementary Figure S4E). This indicates that the observed CAF-1 effect cannot be generalized to

other PIP-containing proteins and that simple PIP-binding competition does not explain the differential CAF-1 effect on the DNA polymerases. Therefore, we concluded that differences in PCNA binding affinities between the two polymerases do not solely explain the differences in their crosstalk to CAF-1, and we propose that additional (e.g. steric) effects by CAF-1 may play a role in the specific Pole inhibition. Together, these results support a model in which CAF-1 differentially affects DNA synthesis by the replicative polymerases on the two daughter strands.

Pole function and interplay with CAF-1 are independent of histone binding

During DNA replication in cells, Pole and CAF-1 both bind H3–H4 (73,82–83). Thus, we set out to test whether histones regulate the crosstalk between CAF-1 and the DNA polymerases on PCNA.

First, we used fluorescence polarization assays to determine the binding affinity of Pole for H3–H4 and found that Pole binds H3–H4 with a K_d of 28 nM. This is a 25 times lower affinity than that of CAF-1 ($K_d = 1.1$ nM) (Supplementary Figure S5A). Nevertheless, this would be sufficient to efficiently bind histones in our assay, where Pole is present at 120 nM. Pol δ has background binding to H3–H4 ($K_d \geq 300$ nM), similarly to RPA which is also present in the reactions ($K_d \geq 300$ nM) (Supplementary Figure S5A). These data show that Pole and CAF-1 efficiently bind H3–H4, while Pol δ and RPA do not bind histones in our assays.

To test the effect of histone binding in the crosstalk between CAF-1 and the DNA polymerases, we pre-incubated either the DNA polymerase or CAF-1 with H3–H4 and monitored how this affected DNA synthesis in primer extension assays. Pole activity was not affected by the addition of H3–H4 (Figure 5A) and the CAF-1-dependent inhibition of Pole was also largely unaffected by the presence of H3–H4 (Figure 5A). As expected, the addition of histones to reactions containing Pol δ had no effect on DNA synthesis or on its crosstalk with CAF-1 (Figure 5B). These data demonstrate that histones do not alter the differential effects that CAF-1 has on Pol δ and Pole via PCNA. This is in line with the limited role of histones in regulating the CAF-1–PCNA interaction on DNA (Figures 1, 3F and Supplementary Figure S3B), confirming that DNA is a dominant effector of the CAF-1–PCNA interaction and thus of the CAF-1 interplay with DNA synthesis. Together, this argues that the effects of CAF-1 on the DNA polymerases is relevant during chromatin assembly at replication forks when histones are bound to the histone chaperones.

Previous studies have shown that CAF-1, Pole and RPA can assemble chromatin during DNA replication (54,82–84). As these proteins are all present in our assays, we set out to directly test which of these histone chaperones can assemble nucleosomes in these reconstitutions. To this end, we combined primer extension reactions with NAQ-based readouts to measure histone deposition (i.e. nucleosome assembly). Because in this assay the substrate is RPA-coated single-stranded DNA, nucleosome formation occurs only after DNA synthesis. In the absence of CAF-1, Pole containing reactions show background levels of nucleosome as-

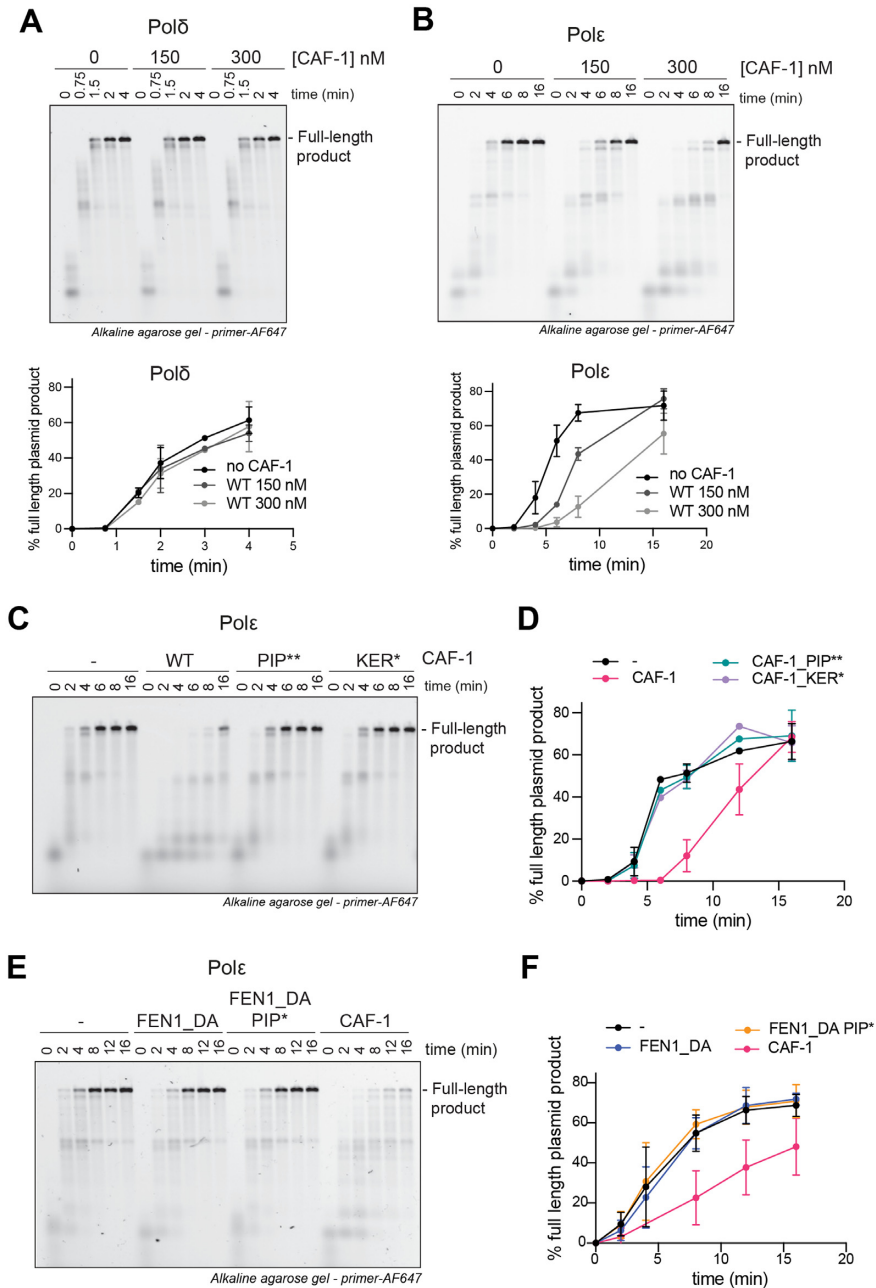


Figure 4. CAF-1 competes with Pol ϵ , not with Pol δ , for PCNA binding. (A, B) (Top) Fluorescence scan of a denaturing alkaline agarose gel of primer extension reactions with Pol δ (A) or Pol ϵ (B). The fluorescently labeled primer signal is shown. The polymerases were at 120 nM, PCNA 480 nM and CAF-1 concentrations as shown. (Bottom) Quantification of the full-length product band relative to the total fluorescence in each lane (expressed as percentages) from the top panels. Mean \pm SD are shown for independent experiments (Pol δ $n = 2$ – Pol ϵ $n = 4$). (C) Fluorescence scan of denaturing alkaline agarose gel of primer extension reactions with Pol ϵ with CAF-1_PIP** and CAF-1_KER* mutants (300 nM). (D) Quantification of primer extension by Pol ϵ in the presence of CAF-1 mutants. Mean \pm SD are shown for three independent experiments. (E) Fluorescence scan of denaturing alkaline agarose gel of primer extension reactions with Pol ϵ with FEN1_DA, FEN1_DA_PIP* and CAF-1 (300 nM). (F) Quantification of primer extension by Pol ϵ in the presence of FEN1_DA and its PIP* mutant version. Mean \pm SD are shown for three independent experiments.

sembly (Figure 5C). These levels are even lower than the histone deposition that we observe with Pol δ , which we used as a negative control because it can synthesize DNA but does not bind histones (Figure 5C). Both reactions contain RPA, indicating that this complex also does not stimulate nucleosome assembly in these primer extension conditions. However, the addition of CAF-1 strongly increases

nucleosome assembly in both conditions (Figure 5C). Similar results were observed when we measure nucleosome assembly on double-stranded DNA fragments using each histone chaperone complex in isolation (Supplementary Figure S5B), which shows that only CAF-1 can stimulate nucleosome assembly. Together, our data demonstrates that Pol ϵ and RPA are not intrinsically capable of nucleosome

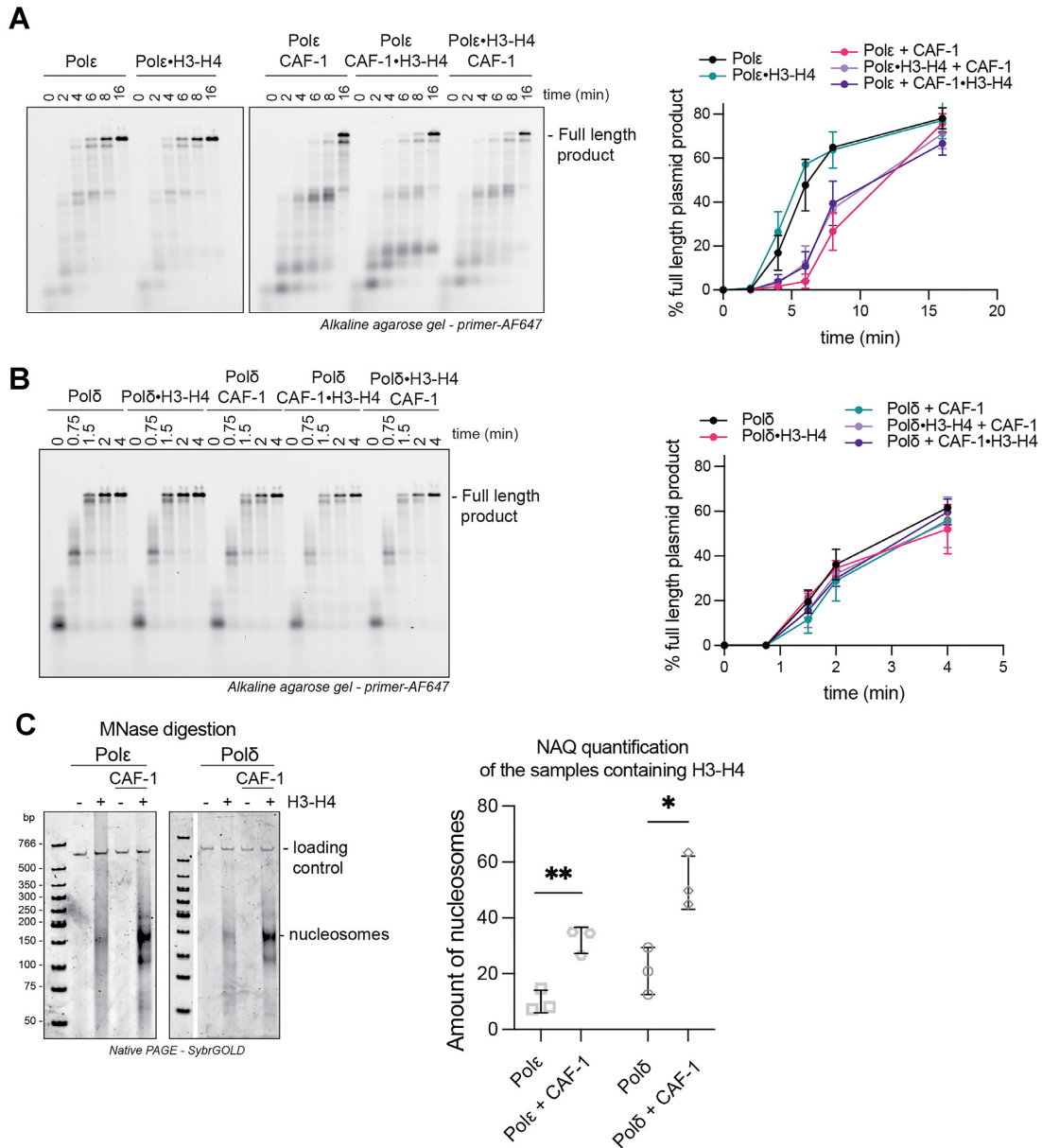


Figure 5. Pole function and interplay with CAF-1 are independent of histone binding. (A, B) (Left) Fluorescence scan of denaturing alkaline agarose gel of primer extension reactions with Pole (A) or Polδ (B) in the presence of H3–H4. H3–H4 were either preincubated with the DNA polymerase or with CAF-1, as indicated by the •. The fluorescently labelled primer signal is shown. (Right) Quantification of primer extension by Pole (A) and Polδ (B) in presence of histones. Mean and SD is shown for three independent experiments. (C) (Left) Native PAGE stained with SybrGOLD to detect protected DNA fragments following MNase digestion during primer extension reactions with Pole or Polδ in presence of CAF-1. H3–H4 were co-incubated with the polymerase or with CAF-1 throughout the reaction, H2A–H2B were added before treatment with 80 units MNase. (Right) Bioanalyzer-based quantification of protected nucleosomal fragments from samples on the left, relative to the loading control band in each lane. Mean ± SD is shown for three independent experiments. * $P < 0.05$, ** $P > 0.01$ (unpaired t-test comparing Pole or Polδ to the condition containing CAF-1).

assembly in a replication-coupled manner, suggesting the main histone deposition factor in these reconstitutions is CAF-1.

CAF-1 deposits newly synthesized H3–H4 on both daughter strands in cells

We identified a differential crosstalk of CAF-1 with Pole and Polδ, likely through their differential interaction with PCNA. As CAF-1 and Pole compete for binding on PCNA,

we wondered whether CAF-1 is able to assemble nucleosomes on the leading strand. To address this question directly in cells, we used mouse embryonic stem cells (mESCs) and employed Sister Chromatid after Replication Sequencing (SCAR-seq) (68,69). This is a genomic method that measures relative protein abundance on the two newly replicated daughter DNA strands, which allowed us to investigate whether depletion of CAF-1 results in a bias in deposition of new histones towards the leading strand.

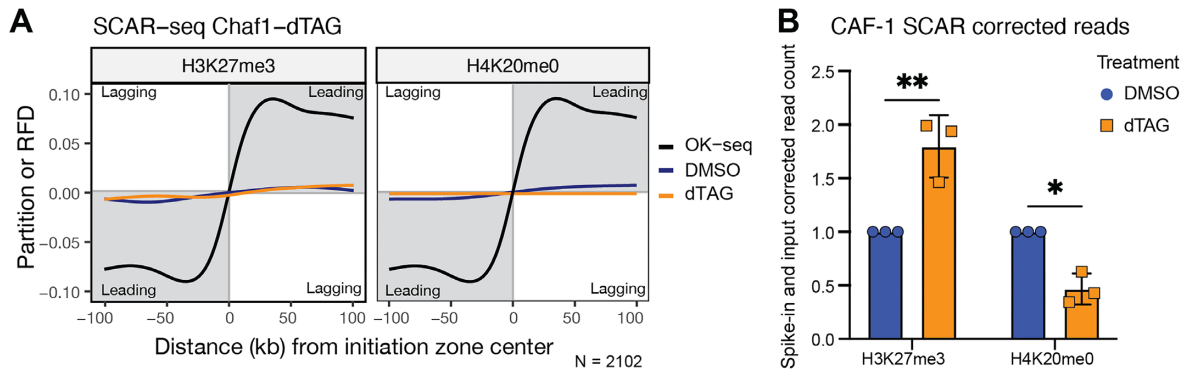


Figure 6. CAF-1 deposits newly synthesized H3–H4 on both leading and lagging strands. (A) Average SCAR-Seq profile of parental (H3K27me3) (left) or newly synthesized (H4K20me0) (right) histones across all replication initiation zones (N(IZ) = 2102) in control (DMSO) or dTAG treated samples. Partition is calculated as the proportion of forward (F) and reverse (R) read counts. Replication fork directionality (RFD) in WT cells measured by Okazaki fragment sequencing (OK-Seq) is shown for comparison. (B) Spike-in normalized values for parental (H3K27me3) and new (H4K20me0) histone modification shows a significant reduction in H4K20me0 samples when CAF-1 is depleted. $n = 3$ independent experiments. * $P < 0.05$, ** $P < 0.01$ (two-way ANOVA).

We first generated a mESC line expressing a CAF-1 p150 subunit that is N-terminally tagged with FKBP12 (named dTAG-*Chaf1a*). dTAG-*Chaf1a* is targeted for proteasomal degradation in the presence of the degrader compound dTAG (85). In these cells, CAF-1 p150 is degraded within 1–2 hours of dTAG treatment (Supplementary Figure S6A), allowing acute depletion of CAF-1 during DNA replication to study its function with minimal pleiotropic effects. We observed that CAF-1 degradation led to a marked reduction of new histones, identified by H4 unmethylated at lysine 20 (H4K20me0), and DNA synthesis, recapitulating known effects of CAF-1 insufficiency (Supplementary Figure S6B–E) (35–36,86–87).

Parental H3–H4 are recycled in a quasi-symmetrical fashion at replication forks, where each newly replicated DNA strand receives about 50% of these histones (68,83). Simultaneously, newly synthesized histones are also symmetrically assembled on the two daughter strands to maintain nucleosome density on replicated DNA (68,83). Control SCAR-seq experiments in untreated dTAG-*Chaf1a* mESCs confirmed these observations, using H3K27me3 as a marker of parental histones (23) and H4K20me0 to mark new histones (88,89) (Figure 6A). Upon dTAG treatment, the total reads in the EdU inputs decreased, consistent with reduced DNA synthesis (Supplementary Figure S6F). Moreover, we observed a 2-fold reduction in reads for the H4K20me0 pulldown upon CAF-1 depletion (Figure 6B), with the H3K27me3-marked parental histones showing a comparable increase (Figure 6B). This could be due to increased MNase accessibility or to effects on parental histones dynamics. This demonstrates that CAF-1 is required for deposition of newly synthesized histones, while parental histone recycling occurs independently of CAF-1. Consistently, parental histones were distributed nearly symmetrically to both daughter strands in the absence of CAF-1 (Figure 6A). Moreover, depletion of CAF-1 did not result in an asymmetric distribution of the new histones that were deposited in this context. This argues that CAF-1 is active on both the leading and lagging strands of active replication forks in mESCs, as are backup systems such as HIRA-dependent gap filling (90).

Together, these data show that CAF-1 functions on both the leading and lagging strand of replication forks in mESCs, where it primarily deposits newly synthesized histones. CAF-1 removal affects the incorporation of these histones on both daughter strands equally without challenging parental histone recycling. This indicates that although CAF-1 and Pole compete for PCNA, both machineries efficiently function on the leading strand.

CAF-1 and Pole compete for PCNA within the replisome

As both CAF-1 and Pole function on the leading strand, we used biochemical reconstitutions to investigate the role of replisome proteins in the interplay between CAF-1 and Pole. Pole is an integral and essential component of the CMG complex at replication forks (10,16–17,91–92). We purified the yeast replisome components that were previously shown to recapitulate physiological DNA replication *in vitro* (8,9) (Supplementary Figure S7A). Our preparations are active as they promote replication of ARS1-containing DNA plasmids in a manner that depends on the presence of the Dbf4-dependent kinase (DDK) (Supplementary Figure S7B) (9).

To focus on Pole activity, we used a pulse-chase setup in which we omitted Pol δ . This allowed us to quantify replication rates of the leading strand only (9), by monitoring replication rates (methods and Supplementary Figure S7B, C). In this assay, Pole is capable of DNA synthesis in the absence of PCNA with a rate of ~ 0.47 kb/min (Figure 7A–C) (9). The addition of PCNA and its loader RFC increases the rate to ~ 1.09 kb/min, recapitulating physiological speeds (Figure 7A–C) (9). Strikingly, the addition of CAF-1 led to a reduction in the rate to ~ 0.85 kb/min (Figure 7A–C), suggesting an inhibitory effect of CAF-1 towards Pole in the context of an active replisome. Consistently, the CAF-1_{PIP**} mutant did not reduce the speed of DNA replication (Figure 7A–C), confirming that this effect is PCNA-dependent. Moreover, a different PIP-containing protein (i.e. FEN1_{DA}) displayed no effect on Pole replication speed within the replisome (Figure 7D–F), suggesting that the observed PCNA-dependent effect of CAF-1 is not

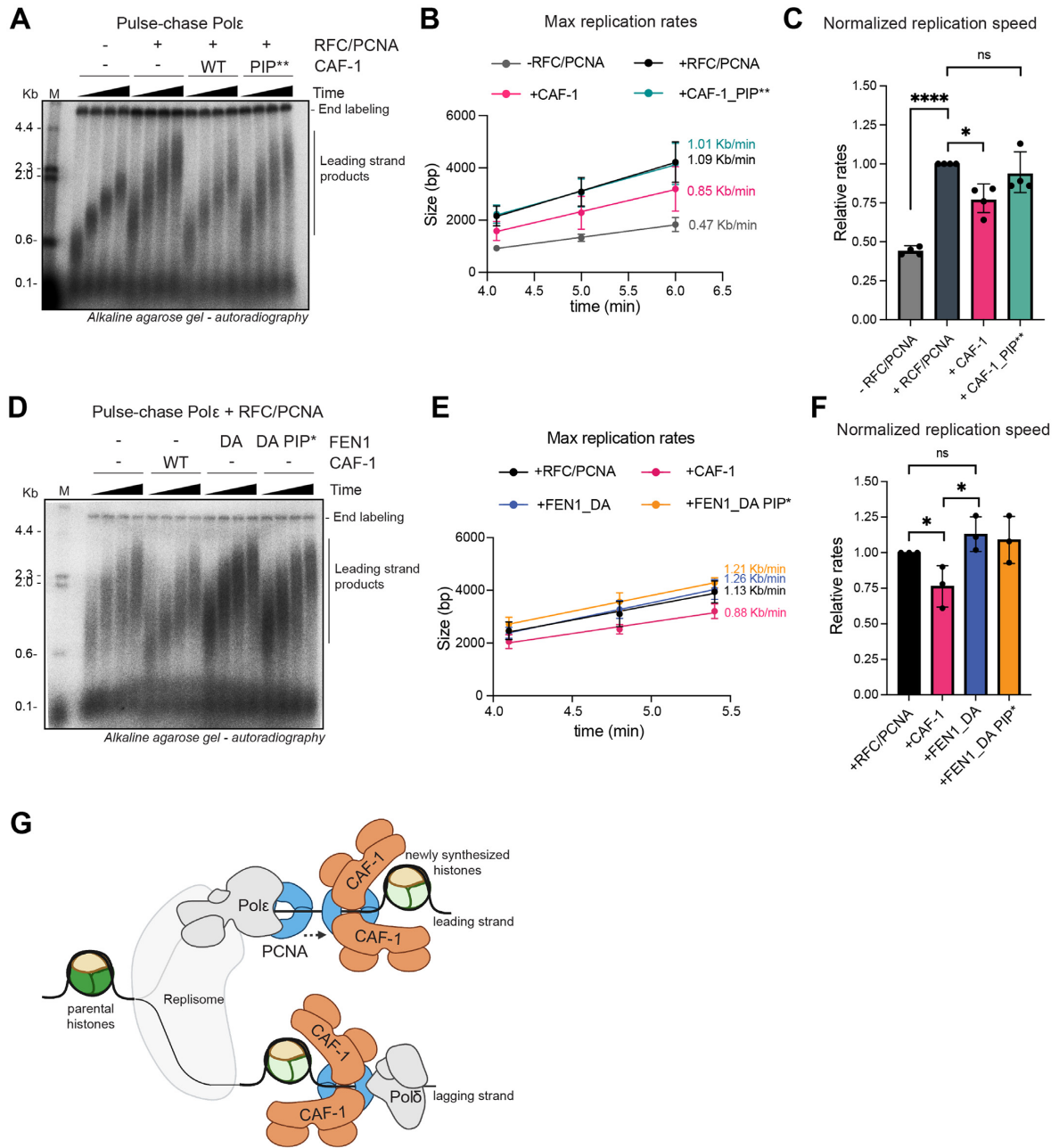


Figure 7. CAF-1 and Polε compete for PCNA binding within the replisome. (A) Autoradiography scan of a denaturing agarose gel of DNA replication products from a pulse-chase experiment in presence of the yeast replisome (Polδ and TopoII are omitted), to test the PCNA-dependent effect of CAF-1 on Pole. All proteins were present during the pulse step (3 min 20 seconds). After addition to the chase solution, reactions were stopped at the indicated time points (4, 5, 6 and 7 min). (B) Quantification of the maximum replication fork rate for pulse-chase experiments in A. Data are shown as mean ± SD of four independent experiments. (C) Graph of normalized replication rates in relation to the + RFC/PCNA sample for each repeat. n = 4 independent experiments. * $P < 0.05$, **** $P < 0.0001$, ns = not significant (one-way ANOVA). (D) Autoradiography scan of a denaturing agarose gel of DNA replication products from a pulse-chase experiment in presence of the yeast replisome (Polδ and TopoII are omitted), to test the PCNA-dependent effect of CAF-1 and FEN1_DA on Pole. All proteins were present during the pulse step (3 min 20 s). After addition to the chase solution, reactions were stopped at the indicated time points (4, 4.8 and 5.4 min). (E) Quantification of the maximum replication fork rate for pulse-chase experiments in (D). Data are shown as mean ± SD of three independent experiments. (F) Graph of normalized replication rates in relation to the + RFC/PCNA sample for each repeat. n = 3 independent experiments. * $P < 0.05$, ns = not significant (unpaired *t*-test). (G) The crosstalk of CAF-1 mediated nucleosome assembly with the DNA replication machinery differs between the leading and lagging strand of replication forks. Two CAF-1 complexes associate with PCNA on DNA to assemble a nucleosome. CAF-1 competes with the leading strand DNA polymerase Pole for PCNA binding, but not with the lagging strand polymerase Polδ. Nevertheless, CAF-1 deposits newly synthesized histones on both daughter strands. This means that on the leading strand, chromatin assembly by CAF-1 cannot occur on the same PCNA that is occupied by Pole. On the lagging strand, CAF-1 may share PCNA with Polδ, but other scenarios could also be envisioned. A direct isolation of the CAF-1-PCNA-Polδ complex is required to prove this hypothesis. The model was created with BioRender.com.

due to an unspecific effect on the availability of binding sites on PCNA.

Together, these data, combined with the observation that CAF-1 acts on both daughter strands (Figure 6A), support a competition between CAF-1 and Pole on PCNA may occur at physiological replication forks, with potential consequences for the control of replication speed of active CMG-Pole complexes.

DISCUSSION

Our work provides insights into how the essential histone chaperone CAF-1 functions during genome replication. We show that CAF-1 recruitment and its PCNA-dependent nucleosome assembly activity are regulated by a complex set of interactions between CAF-1 and PCNA, DNA and histones. Our results argue that several structural transitions regulate CAF-1, and we anticipate that these control the timing of CAF-1 arrival to, action on and departure from replication forks. This is linked with the interplay between CAF-1, PCNA and the DNA polymerases. CAF-1 competes with Pole for PCNA binding, while it has no effect on Pol δ . Yet, CAF-1 deposits newly synthesized histones equally on both strands in mESCs. Therefore, the competition between CAF-1 and Pole appears to be an integrated part of coordinating replication and nucleosome assembly and does not limit CAF-1 function. Our work suggests that different mechanisms are in place on the leading and lagging strand to couple DNA synthesis with CAF-1 mediated nucleosome assembly, in line with the inherent asymmetry of DNA replication and its chromatin assembly mechanisms.

CAF-1 effects on DNA synthesis on the two daughter strands

On the leading strand, we propose that CAF-1 and Pole either interact with distinct PCNA clamps or that they dynamically alternate in binding to PCNA, due to their competition (Figure 7G). The first model argues for a controlled spatial separation between DNA synthesis and chromatin assembly, raising questions on how this is enforced at replication forks where all these factors are enriched at the same site and nucleosomes are assembled almost immediately after DNA synthesis (93,94). The second model instead evokes an attractive PCNA hand-off mechanism between Pole and CAF-1. In this mechanism, only when enough DNA has been synthesized by Pole (± 30 bp, Figure 1G), CAF-1 is recruited and its arrival destabilizes Pole from PCNA (Figure 4B) (15,95). This allows CAF-1 to use PCNA for nucleosome assembly, and a new PCNA must be loaded for Pole to proceed with leading strand synthesis (19). This mechanism may enable continued PCNA loading on the leading strand during elongation (19), and the immediate coupling of chromatin assembly on newly replicated DNA (21–22,93–94). It is also interesting to note that this molecular interplay could have direct effects on the speed of leading-strand DNA synthesis *in vivo*. Both models imply the need for regulatory steps in PCNA accessibility and loading on the leading strand, where the CTF18 clamp loader that binds Pole may well play a role (19,96).

On the lagging strand, CAF-1 does not affect Pol δ activity (Figure 4A). Since Pol δ occupies only one of the PCNA

monomers on the DNA-loaded clamp (97,98) (Supplementary Figure S7D), and it allows binding of other PIP containing proteins (i.e. FEN1)(97), we speculate that CAF-1 and Pol δ may share the same PCNA clamp (Figure 7G). This is also consistent with cellular evidence that closely links Okazaki fragments size with nucleosome assembly by CAF-1 (54,99). However, a direct isolation of the CAF-1–PCNA–Pol δ complex is required to conclusively prove this hypothesis. It will be further interesting to investigate how CAF-1 affects the Pol δ -dependent activities on the leading strand (9,100).

De novo chromatin assembly during DNA replication

We show that CAF-1 primarily deposits newly synthesized histones H3–H4 equally on both daughter strands in cells (Figure 6). As Pole is a histone chaperone for parental H3–H4 (82,83), the competition between CAF-1 and Pole on PCNA may further control the alternation of parental and new histones incorporation on newly replicated leading strand DNA. Interestingly, we did not detect histone deposition activity by Pole in our assays, indicating that additional factors may be functioning on the leading strand to promote parental nucleosome assembly. On the lagging strand instead, as Pol δ does not have histone chaperone activity (Supplementary Figure S5A), CAF-1 may be required to be in close proximity to assemble chromatin. However, this activity needs to intercalate with parental histone deposition, for which the responsible histone chaperone still needs to be clearly defined. RPA is a good candidate (84) but we observe no activity for this complex in our primer extension assays. DNA polymerase alpha (Pol α) histone-binding is required for parental histone recycling to lagging strand (101–103), but it remains unclear how it could deposit histones in relation to PCNA loading and Pol δ function.

Interestingly, this and previous work highlight that CAF-1 does not strictly require PCNA for nucleosome assembly (Figure 2) (54,75). This suggests that CAF-1 may use PIP-independent activities at replication forks after the initial PCNA-dependent recruitment, which should be considered when building models of chromatin assembly during DNA replication. To unravel these mechanisms, biochemical reconstitutions with integrated readouts for DNA synthesis and chromatin assembly at high spatial and time resolution, together with the use of CAF-1 separation-of-function mutants are required. Our work provides tools to build such complex reconstitutions, which will enable a complete understanding of how parental and new histone deposition pathways are integrated during ongoing DNA replication.

DATA AVAILABILITY

Fastaq files from MNase-seq are uploaded to OSF and can be accessed with the following link:

https://osf.io/2vd4z/?view_only=5ffa1e0b749445da9b22a11577f3d47f

SCAR-seq data are available with GEO accession GSE223782 (<https://www.ncbi.nlm.nih.gov/geo/query/acc.cgi?acc=GSE223782>)

SUPPLEMENTARY DATA

Supplementary Data are available at NAR Online.

ACKNOWLEDGEMENTS

We thank John Diffley, Peter Burgers, Xiaodong Zhang, Rafael Fernández Leiro and Zhihao Zhuang for sharing reagents, Titia Sixma and Shreya Dharadhar for help with RFC Δ N purification, Juan Garaycoechea for discussions and critical reading of the manuscript, Anke Sparmann at Life Science Editors for editing services (www.lifescienceeditors.com), Jamie Barnett for designing and sharing primers for NGS, Jan Dreyer for discussions on the PCNA-NAQ assay, The Histone Source at Colorado State University for lyophilized histones, and the CPR/ReNew Genomics platform.

Authors contributions: Conceptualization: C.R., B.V.E., L.K., A.G., F.M.; Data Curation: C.R., B.V.E., L.K., F.G., F.M.; Formal Analysis: C.R., B.V.E., L.K., F.G., A.E.E.V., I.R., P.H.L.K., F.M.; Funding acquisition: A.G., F.M.; Investigation: C.R., B.V.E., L.K., F.G., A.E.E.V., I.R., G.R., P.A., F.M.; Methodology: C.R., B.V.E., L.K., F.G., A.E.E.V., I.R., A.B., T.v.L., P.A., K.S., F.M.; Project administration: F.M.; Software: P.H.L.K.; Supervision: R.A.S., W.d.L., P.K., N.H.D., A.G., F.M.; Validation: C.D.v.F., G.L.; Visualization: C.R., B.V.E., L.K., F.G., F.M.; Writing – original draft: C.R., B.V.E., F.M.; Writing – Review & Editing: all authors.

FUNDING

F.M. is funded by the Dutch Cancer Society [KWF 2014-6649]; European Union [ERC-StG 851564]; A.G. is supported by the European Research Council [ERC CoG 724436]; Lundbeck Foundation[R198-2015-269, R313-2019-448]; Independent Research Fund Denmark [7016-00042B]; Novo Nordisk Foundation [NNF14OC0012839]; research at CPR is supported by the Novo Nordisk Foundation [NNF14CC0001]; A.B. was supported by Marie Curie Individual Fellowship [841620]; N.D. acknowledges funding from the Netherlands Organisation for Scientific Research (NWO) through Top grant [714.017.002]; European Research Council through an Advanced Grant [REPLICHROMA; 789267]; R.A.S. is funded through the European Union Horizon 2020 program INFRAIA project Epic-XS [823839]; research program NWO TA [741.018.201], which is partly financed by NWO; P.K. was supported by the European Research Council (ERC) through an ERC Consolidator Grant [ERCCOG 101003210-XlinkRepair]; Oncode Institute, which is partly financed by the Dutch Cancer Society (KWF); K.S. was supported by the Japanese Biochemical Society through the Osamu Hayaishi Memorial Scholarship for Study Abroad. Funding for open access charge: ERC [StG 851564].

Conflict of interest statement. A.G. is cofounder and chief scientific officer (CSO) of Ankrin Therapeutics. The authors declare no competing interests.

REFERENCES

- Bellelli, R. and Boulton, S.J. (2021) Spotlight on the replisome: aetiology of DNA replication-associated genetic diseases. *Trends Genet.*, **37**, 317–336.
- Escobar, T.M., Loyola, A. and Reinberg, D. (2021) Parental nucleosome segregation and the inheritance of cellular identity. *Nat. Rev. Genet.*, **22**, 379–392.
- Hills, S.A. and Diffley, J.F.X. (2014) DNA replication and oncogene-induced replicative stress. *Curr. Biol.*, **24**, R435–R444.
- Stewart-Morgan, K.R., Petryk, N. and Groth, A. (2020) Chromatin replication and epigenetic cell memory. *Nat. Cell Biol.*, **22**, 361–371.
- Bell, S.P. and Labib, K. (2016) Chromosome duplication in *Saccharomyces cerevisiae*. *Genetics*, **203**, 1027–1067.
- Pellegrini, L. and Costa, A. (2016) New insights into the mechanism of DNA duplication by the eukaryotic replisome. *Trends Biochem. Sci.*, **41**, 859–871.
- Li, H. and O'Donnell, M.E. (2018) The eukaryotic CMG helicase at the replication fork: emerging architecture reveals an unexpected mechanism. *Bioessays*, **40**, 1700208.
- Yeeles, J.T.P., Deegan, T.D., Janska, A., Early, A. and Diffley, J.F.X. (2015) Regulated eukaryotic DNA replication origin firing with purified proteins. *Nature*, **519**, 431–435.
- Yeeles, J.T.P., Janska, A., Early, A. and Diffley, J.F.X. (2017) How the eukaryotic replisome achieves rapid and efficient DNA replication. *Mol. Cell*, **65**, 105–116.
- Langston, L.D., Zhang, D., Yurieva, O., Georgescu, R.E., Finkelstein, J., Yao, N.Y., Indiani, C. and O'Donnell, M.E. (2014) CMG helicase and DNA polymerase ϵ form a functional 15-subunit holoenzyme for eukaryotic leading-strand DNA replication. *Proc. Natl. Acad. Sci. U.S.A.*, **111**, 15390–15395.
- Zhou, J.C., Janska, A., Goswami, P., Renault, L., Abid Ali, F., Kotecha, A., Diffley, J.F.X. and Costa, A. (2017) CMG-Pol epsilon dynamics suggests a mechanism for the establishment of leading-strand synthesis in the eukaryotic replisome. *Proc. Natl. Acad. Sci. U.S.A.*, **114**, 4141–4146.
- Nick McElhinny, S.A., Gordenin, D.A., Stith, C.M., Burgers, P.M.J. and Kunkel, T.A. (2008) Division of labor at the eukaryotic replication fork. *Mol. Cell*, **30**, 137–144.
- Burgers, P.M.J. and Kunkel, T.A. (2017) Eukaryotic DNA replication fork. *Annu. Rev. Biochem.*, **86**, 417–438.
- Guilliam, T.A. and Yeeles, J.T.P. (2020) An updated perspective on the polymerase division of labor during eukaryotic DNA replication. *Crit. Rev. Biochem. Mol. Biol.*, **55**, 469–481.
- Chilkova, O., Stenlund, P., Isoz, L., Stith, C.M., Grabowski, P., Lundstrom, E.-B., Burgers, P.M. and Johansson, E. (2007) The eukaryotic leading and lagging strand DNA polymerases are loaded onto primer-ends via separate mechanisms but have comparable processivity in the presence of PCNA. *Nucleic Acids Res.*, **35**, 6588–6597.
- Georgescu, R.E., Langston, L., Yao, N.Y., Yurieva, O., Zhang, D., Finkelstein, J., Agarwal, T. and O'Donnell, M.E. (2014) Mechanism of asymmetric polymerase assembly at the eukaryotic replication fork. *Nat. Struct. Mol. Biol.*, **21**, 664–670.
- Schauer, G.D. and O'Donnell, M.E. (2017) Quality control mechanisms exclude incorrect polymerases from the eukaryotic replication fork. *Proc. Natl. Acad. Sci. U.S.A.*, **114**, 675–680.
- Moldovan, G.L., Pfander, B. and Jentsch, S. (2007) PCNA, the maestro of the replication fork. *Cell*, **129**, 665–679.
- Liu, H.W., Bouchoux, C., Panarotto, M., Kakui, Y., Patel, H. and Uhlmann, F. (2020) Division of labor between PCNA loaders in DNA replication and sister chromatid cohesion establishment. *Mol. Cell*, **78**, 725–738.
- Yu, C., Gan, H., Han, J., Zhou, Z.X., Jia, S., Chabes, A., Farrugia, G., Ordog, T. and Zhang, Z. (2014) Strand-specific analysis shows protein binding at replication forks and PCNA unloading from lagging strands when forks stall. *Mol. Cell*, **56**, 551–563.
- Sogo, J.M., Stahl, H., Koller, T. and Knippers, R. (1986) Structure of replicating simian virus 40 minichromosomes. *J. Mol. Biol.*, **189**, 189–204.
- McKnight, S.L. and Miller, O.L. (1977) Electron microscopic analysis of chromatin replication in the cellular blastoderm *Drosophila melanogaster* embryo. *Cell*, **12**, 795–804.

23. Alabert,C., Barth,T.K., Reverón-Gómez,N., Sidoli,S., Schmidt,A., Jensen,O.N., Imhof,A. and Groth,A. (2015) Two distinct modes for propagation of histone ptms across the cell cycle. *Genes Dev.*, **29**, 585–590.
24. Stewart-Morgan,K.R., Reverón-Gómez,N. and Groth,A. (2019) Transcription restart establishes chromatin accessibility after DNA replication. *Mol. Cell*, **75**, 284–297.
25. Escobar,T.M., Oksuz,O., Saldañ A-Meyer,R., Descostes,N., Bonasio,R. and Correspondence,D.R. (2019) Active and repressed chromatin domains exhibit distinct nucleosome segregation during DNA replication. *Cell*, **179**, 953–963.
26. Ramachandran,S. and Henikoff,S. (2016) Transcriptional regulators compete with nucleosomes post-replication. *Cell*, **165**, 580–592.
27. Franklin,R., Murn,J. and Cheloufi,S. (2021) Cell fate decisions in the wake of histone H3 deposition. *Front. Cell Dev. Biol.*, **9**, 654915.
28. Smith,S. and Stillman,B. (1989) Purification and characterization of CAF-I, a human cell factor required for chromatin assembly during DNA replication in vitro. *Cell*, **58**, 15–25.
29. Houliard,M., Berlivet,S., Probst,A.v., Quivy,J.P., Héry,P., Almouzni,G. and Gérard,M. (2006) CAF-1 is essential for heterochromatin organization in pluripotent embryonic cells. *PLoS Genet.*, **2**, 1686–1696.
30. Song,Y., He,F., Xie,G., Guo,X., Xu,Y., Chen,Y., Liang,X., Stagljar,I., Egli,D., Ma,J. *et al.* (2007) CAF-1 is essential for Drosophila development and involved in the maintenance of epigenetic memory. *Dev. Biol.*, **311**, 213–222.
31. Fischer,S., Prykhodzhiy,S., Rau,M.J. and Neumann,C.J. (2007) Mutation of zebrafish caf-1b results in S phase arrest, defective differentiation and p53-mediated apoptosis during organogenesis. *Cell Cycle*, **6**, 2962–2969.
32. Cheloufi,S., Elling,U., Hopfgartner,B., Jung,Y.L., Murn,J., Ninova,M., Hubmann,M., Badeaux,A.I., Euong Ang,C., Tenen,D. *et al.* (2015) The histone chaperone CAF-1 safeguards somatic cell identity. *Nature*, **528**, 218–224.
33. Franklin,R., Guo,Y., He,S., Chen,M., Ji,F., Zhou,X., Frankhouser,D., Do,B.T., Chiem,C., Jang,M. *et al.* (2022) Regulation of chromatin accessibility by the histone chaperone CAF-1 sustains lineage fidelity. *Nat. Commun.*, **13**, 2350.
34. Ye,X., Franco,A.A., Santos,H., Nelson,D.M., Kaufman,P.D. and Adams,P.D. (2003) Defective S phase chromatin assembly causes DNA damage, activation of the S phase checkpoint, and S phase arrest. *Mol. Cell*, **11**, 341–351.
35. Hoek,M. and Stillman,B. (2003) Chromatin assembly factor 1 is essential and couples chromatin assembly to DNA replication in vivo. *Proc. Natl. Acad. Sci. U.S.A.*, **100**, 12183–12188.
36. Quivy,J.-P.P., Gérard,A., Cook,A.J.L.L., Roche,D. and Almouzni,G. (2008) The HP1-p150/CAF-1 interaction is required for pericentric heterochromatin replication and S-phase progression in mouse cells. *Nat. Struct. Mol. Biol.*, **15**, 972–979.
37. Gaillard,P.H.L., Martini,E.M.D., Kaufman,P.D., Stillman,B., Moustacchi,E. and Almouzni,G. (1996) Chromatin assembly coupled to DNA repair: a new role for chromatin assembly factor I. *Cell*, **86**, 887–896.
38. Cheng,L., Zhang,X., Wang,Y., Gan,H., Xu,X., Lv,X., Hua,X., Que,J., Ordog,T. and Zhang,Z. (2019) Chromatin Assembly Factor 1 (CAF-1) facilitates the establishment of facultative heterochromatin during pluripotency exit. *Nucleic Acids Res.*, **47**, 11114–11131.
39. Polo,S.E., Theocharis,S.E., Kljanienco,J., Savignoni,A., Asselain,B., Vielh,P. and Almouzni,G. (2004) Chromatin assembly factor-1, a marker of clinical value to distinguish quiescent from proliferating cells. *Cancer Res.*, **64**, 2371–2381.
40. Volk,A., Liang,K., Suraneni,P., Li,X., Zhao,J., Bulic,M., Marshall,S., Pulakanti,K., Malinge,S., Taub,J. *et al.* (2018) A CHAF1B-dependent molecular switch in hematopoiesis and leukemia pathogenesis. *Cancer Cell*, **34**, 707–723.
41. Barbieri,E., de Preter,K., Capasso,M., Chen,Z., Hsu,D.M., Tonini,G.P., Lefever,S., Hicks,J., Versteeg,R., Pession,A. *et al.* (2014) Histone chaperone CHAF1A inhibits differentiation and promotes aggressive neuroblastoma. *Cancer Res.*, **74**, 765–774.
42. Zhang,Z., Shibahara,K.I. and Stillman,B. (2000) PCNA connects DNA replication to epigenetic inheritance in yeast. *Nature*, **408**, 221–225.
43. Almouzni,G., Clark,D.J., Méchali,M. and Wolffe,A.P. (1990) Chromatin assembly on replicating DNA in vitro. *Nucleic Acids Res.*, **18**, 5767–5774.
44. Smith,S. and Stillman,B. (1991) Immunological characterization of chromatin assembly factor I, a human cell factor required for chromatin assembly during DNA replication in vitro. *J. Biol. Chem.*, **266**, 12041–12047.
45. Kaufman,P.D., Kobayashi,R. and Stillman,B. (1997) Ultraviolet radiation sensitivity and reduction of telomeric silencing in Saccharomyces cerevisiae cells lacking chromatin assembly factor-I. *Genes Dev.*, **11**, 345–357.
46. Kaufman,P.D., Kobayashi,R., Kessler,N. and Stillman,B. (1995) The p150 and p60 subunits of chromatin assembly factor I: a molecular link between newly synthesized histones and DNA replication. *Cell*, **81**, 1105–1114.
47. Verreault,A., Kaufman,P.D., Kobayashi,R. and Stillman,B. (1996) Nucleosome assembly by a complex of CAF-1 and acetylated histones H3/H4. *Cell*, **87**, 95–104.
48. Shibahara,K.I. and Stillman,B. (1999) Replication-dependent marking of DNA by PCNA facilitates CAF-1-coupled inheritance of chromatin. *Cell*, **96**, 575–585.
49. Moggs,J.G., Grandi,P., Quivy,J.-P., Jonsson,Z.O., Hubscher,U., Becker,P.B. and Almouzni,G. (2000) A CAF-1-PCNA-mediated chromatin assembly pathway triggered by sensing DNA damage. *Mol. Cell Biol.*, **20**, 1206–1218.
50. Gopinathan Nair,A., Rabas,N., Lejon,S., Homiski,C., Osborne,M.J., Cyr,N., Sverzhinsky,A., Melendy,T., Pascal,J.M., Laue,E.D. *et al.* (2022) Unorthodox PCNA Binding by Chromatin Assembly Factor 1. *Int J Mol Sci.*, **23**, 11099.
51. Krawitz,D.C., Kama,T. and Kaufman,P.D. (2002) Chromatin assembly factor I mutants defective for PCNA binding require Asf1/Hir proteins for silencing. *Mol. Cell Biol.*, **22**, 614–625.
52. Tsirkas,I., Dovrat,D., Lei,Y., Kalyva,A., Lotysh,D., Li,Q. and Aharoni,A. (2021) Cac1 WHD and PIP domains have distinct roles in replisome progression and genomic stability. *Curr. Genet.*, **67**, 129–139.
53. Ben-Shahar,T.R., Castillo,A.G., Osborne,M.J., Borden,K.L.B., Kornblatt,J. and Verreault,A. (2009) Two fundamentally distinct PCNA interaction peptides contribute to chromatin assembly factor 1 function. *Mol. Cell Biol.*, **29**, 6353–6365.
54. Mattioli,F., Gu,Y., Yadav,T., Balsbaugh,J.L.J.L., Harris,M.R.M.R., Findlay,E.S.E.S., Liu,Y., Radebaugh,C.A.C.A., Stargell,L.A.L.A., Ahn,N.G.N.G. *et al.* (2017) DNA-mediated association of two histone-bound complexes of yeast chromatin assembly factor-1 (CAF-1) drives tetrasome assembly in the wake of DNA replication. *Elife*, **6**, e22799.
55. Mattioli,F., Gu,Y., Balsbaugh,J.L.J.L., Ahn,N.G.N.G. and Luger,K. (2017) The Cac2 subunit is essential for productive histone binding and nucleosome assembly in CAF-1. *Sci. Rep.*, **7**, 46274.
56. Hibbert,R.G. and Sixma,T.K. (2012) Intrinsic flexibility of ubiquitin on proliferating cell nuclear antigen (PCNA) in translesion synthesis. *J. Biol. Chem.*, **287**, 39216–39223.
57. Muthurajan,U., Mattioli,F., Bergeron,S., Zhou,K., Gu,Y., Chakravarthy,S., Dyer,P., Irving,T. and Luger,K. (2016) In vitro chromatin assembly: strategies and quality control. In: *Methods in Enzymology*. Vol. **573**, pp. 3–41.
58. Dyer,P.N., Edayathumangalam,R.S., White,C.L., Bao,Y., Chakravarthy,S., Muthurajan,U.M. and Luger,K. (2004) Reconstitution of nucleosome core particles from recombinant histones and DNA. *Methods Enzymol.*, **375**, 23–44.
59. Baretic,D., Jenkyn-Bedford,M., Aria,V., Cannone,G., Skehel,M. and Yeeles,J.T.P. (2020) Cryo-EM structure of the fork protection complex bound to CMG at a replication fork. *Mol. Cell*, **78**, 926–940.
60. Chen,J., Ai,Y., Wang,J., Haracska,L. and Zhuang,Z. (2010) Chemically ubiquitylated PCNA as a probe for eukaryotic translesion DNA synthesis. *Nat. Chem. Biol.*, **6**, 270–272.
61. Gomes,X.v., Gary,S.L. and Burgers,P.M.J. (2000) Overproduction in Escherichia coli and characterization of yeast replication factor C lacking the ligase homology domain. *J. Biol. Chem.*, **275**, 14541–14549.
62. Yates,L.A., Aramayo,R.J., Pokhrel,N., Caldwell,C.C., Kaplan,J.A., Perera,R.L., Spies,M., Antony,E. and Zhang,X. (2018) A structural

- and dynamic model for the assembly of Replication Protein A on single-stranded DNA. *Nat. Commun.*, **9**, 5447.
63. Mattioli, F., Gu, Y. and Luger, K. (2018) Measuring nucleosome assembly activity in vitro with the nucleosome assembly and quantification (NAQ) assay. *Bio Protoc.*, **8**, 1–11.
 64. Sato, K., Martin-Pintado, N., Post, H., Altelaar, M. and Knipscheer, P. (2021) Multistep mechanism of G-quadruplex resolution during DNA replication. *Sci. Adv.*, **7**, eabf8653.
 65. Blackledge, N.P., Fursova, N.A., Kelley, J.R., Huseyin, M.K., Feldmann, A. and Klose, R.J. (2020) PRC1 Catalytic activity is central to polycomb system function. *Mol. Cell.*, **77**, 857–874.
 66. Quivy, J.P., Roche, D., Kirschner, D., Tagami, H., Nakatani, Y. and Almouzni, G. (2004) A CAF-1 dependent pool of HP1 during heterochromatin duplication. *EMBO J.*, **23**, 3516–3526.
 67. Hammond, C.M., Bao, H., Hendriks, I.A., Carraro, M., Garcia-Nieto, A., Liu, Y., Reverón-Gómez, N., Spanos, C., Chen, L., Rappilber, J. et al. (2021) DNAJC9 integrates heat shock molecular chaperones into the histone chaperone network. *Mol. Cell.*, **81**, 2533–2548.
 68. Petryk, N., Dalby, M., Wenger, A., Stromme, C.B., Strandsby, A., Andersson, R. and Groth, A. (2018) MCM2 promotes symmetric inheritance of modified histones during DNA replication. *Science (1979)*, **361**, 1389–1392.
 69. Petryk, N., Reverón-Gómez, N., González-Aguilera, C., Dalby, M., Andersson, R. and Groth, A. (2021) Genome-wide and sister chromatid-resolved profiling of protein occupancy in replicated chromatin with ChOR-seq and SCAR-seq. *Nat. Protoc.*, **16**, 4446–4493.
 70. Fursova, N.A., Blackledge, N.P., Nakayama, M., Ito, S., Koseki, Y., Farcas, A.M., King, H.W., Koseki, H. and Klose, R.J. (2019) Synergy between variant PRC1 complexes defines polycomb-mediated gene repression. *Mol. Cell.*, **74**, 1020–1036.
 71. Yoder, B.L. and Burgers, P.M. (1991) *Saccharomyces cerevisiae* replication factor C. I. Purification and characterization of its atpase activity. *J. Biol. Chem.*, **266**, 22689–22697.
 72. Dharadhar, S., Dijk, W.J., Scheffers, S., Fish, A. and Sixma, T.K. (2021) Insert L1 is a central hub for allosteric regulation of USP1 activity. *EMBO Rep.*, **22**, e51749.
 73. Sauer, P.v., Gu, Y., Liu, W.H., Mattioli, F., Panne, D., Luger, K. and Churchill, M.E.A. (2018) Mechanistic insights into histone deposition and nucleosome assembly by the chromatin assembly factor-1. *Nucleic Acids Res.*, **46**, 9907–9917.
 74. Zhang, K., Gao, Y., Li, J., Burgess, R., Han, J., Liang, H., Zhang, Z. and Liu, Y. (2016) A DNA binding winged helix domain in CAF-1 functions with PCNA to stabilize CAF-1 at replication forks. *Nucleic Acids Res.*, **44**, 5083–5094.
 75. Sauer, P.V., Timm, J., Liu, D., Sitbon, D., Boeri-Erba, E., Velours, C., Mücke, N., Langowski, J., Ochsenbein, F., Almouzni, G. et al. (2017) Insights into the molecular architecture and histone H3–H4 deposition mechanism of yeast chromatin assembly factor 1. *Elife*, **6**, 835–839.
 76. Rosas, R., Aguilar, R.R., Arslanovic, N., Tyler, J.K. and Churchill, M.E.A. (2022) A novel Single alpha-Helix-DNA-binding domain in CAF-1 promotes gene silencing and DNA damage survival through tetrasome-length DNA selectivity and spacer function. bioRxiv doi: <https://doi.org/10.1101/2022.10.11.511754>, 11 October 2022, preprint: not peer reviewed.
 77. Liu, W.H., Roemer, S.C., Zhou, Y., Shen, Z.J., Dennehey, B.K., Balsbaugh, J.L., Liddle, J.C., Nemkov, T., Ahn, N.G., Hansen, K.C. et al. (2016) The Cacl subunit of histone chaperone CAF-1 organizes CAF-1-H3/H4 architecture and tetramerizes histones. *Elife*, **5**, 2852–2861.
 78. Young, G., Hundt, N., Cole, D., Fineberg, A., Andrecka, J., Tyler, A., Olerinyova, A., Ansari, A., Marklund, E.G., Collier, M.P. et al. (2018) Quantitative mass imaging of single biological macromolecules. *Science (1979)*, **360**, 423–427.
 79. Mondol, T., Stodola, J.L., Galletto, R. and Burgers, P.M. (2019) PCNA accelerates the nucleotide incorporation rate by DNA polymerase δ . *Nucleic Acids Res.*, **47**, 1977–1986.
 80. Gomes, X.v. and Burgers, P.M.J. (2000) Two modes of FEN1 binding to PCNA regulated by DNA. *EMBO J.*, **19**, 3811–3821.
 81. Dovrat, D., Stodola, J.L., Burgers, P.M.J. and Aharoni, A. (2014) Sequential switching of binding partners on PCNA during in vitro Okazaki fragment maturation. *Proc. Natl. Acad. Sci.*, **111**, 14118–14123.
 82. Bellelli, R., Belan, O., Pye, V.E., Clement, C., Maslen, S.L., Skehel, J.M., Cherepanov, P., Almouzni, G. and Boulton, S.J. (2018) POLE3-POLE4 Is a histone H3–H4 chaperone that maintains chromatin integrity during DNA replication. *Mol. Cell.*, **72**, 112–126.
 83. Yu, C., Gan, H., Serra-Cardona, A., Zhang, L., Gan, S., Sharma, S., Johansson, E., Chabes, A., Xu, R.M. and Zhang, Z. (2018) A mechanism for preventing asymmetric histone segregation onto replicating DNA strands. *Science*, **361**, 1386–1389.
 84. Liu, S., Xu, Z., Leng, H., Zheng, P., Yang, J., Chen, K., Feng, J. and Li, Q. (2017) RPA binds histone H3–H4 and functions in DNA replication-coupled nucleosome assembly. *Science*, **355**, 415–420.
 85. Nabet, B., Roberts, J.M., Buckley, D.L., Paulk, J., Dastjerdi, S., Yang, A., Leggett, A.L., Erb, M.A., Lawlor, M.A., Souza, A. et al. (2018) The dTAG system for immediate and target-specific protein degradation. *Nat. Chem. Biol.*, **14**, 431–441.
 86. Mejlvang, J., Feng, Y., Alabert, C., Neelsen, K.J., Jasencakova, Z., Zhao, X., Lees, M., Sandelin, A., Pasero, P., Lopes, M. et al. (2014) New histone supply regulates replication fork speed and PCNA unloading. *J. Cell Biol.*, **204**, 29–43.
 87. Klapholz, B., Dietrich, B.H., Schaffner, C., Hérédia, F., Quivy, J.P., Almouzni, G. and Dostatni, N. (2009) CAF-1 is required for efficient replication of euchromatic DNA in *Drosophila* larval endocycling cells. *Chromosoma*, **118**, 235–248.
 88. Nakamura, K., Saredi, G., Becker, J.R., Foster, B.M., Nguyen, N.v., Beyer, T.E., Cesa, L.C., Faull, P.A., Lukauskas, S., Frimurer, T. et al. (2019) H4K20me0 recognition by BRCA1–BARD1 directs homologous recombination to sister chromatids. *Nat. Cell Biol.*, **21**, 311–318.
 89. Saredi, G., Huang, H., Hammond, C.M., Alabert, C., Bekker-Jensen, S., Forne, I., Reverón-Gómez, N., Foster, B.M., Mlejnkova, L., Bartke, T. et al. (2016) H4K20me0 marks post-replicative chromatin and recruits the TONSL-MMS22L DNA repair complex. *Nature*, **534**, 714–718.
 90. Ray-Gallet, D., Woolfe, A., Vassias, I., Pellentz, C., Lacoste, N., Puri, A., Schultz, D.C., Pchelintsev, N.A., Adams, P.D., Jansen, L.E.T. et al. (2011) Dynamics of histone H3 deposition in vivo reveal a nucleosome gap-filling mechanism for H3.3 to maintain chromatin integrity. *Mol. Cell.*, **44**, 928–941.
 91. Goswami, P., Abid Ali, F., Douglas, M.E., Locke, J., Purkiss, A., Janska, A., Eickhoff, P., Early, A., Nans, A., Cheung, A.M.C. et al. (2018) Structure of DNA-CMG-Pol epsilon elucidates the roles of the non-catalytic polymerase modules in the eukaryotic replisome. *Nat. Commun.*, **9**, 5061.
 92. Sun, J., Shi, Y., Georgescu, R.E., Yuan, Z., Chait, B.T., Li, H. and O'Donnell, M.E. (2015) The architecture of a eukaryotic replisome. *Nat. Struct. Mol. Biol.*, **22**, 976–982.
 93. Lucchini, R., Wellinger, R.E. and Sogo, J.M. (2001) Nucleosome positioning at the replication fork. *EMBO J.*, **20**, 7294–7302.
 94. Gasser, R., Koller, T. and Sogo, J.M. (1996) The stability of nucleosomes at the replication fork. *J. Mol. Biol.*, **258**, 224–239.
 95. Hogg, M., Osterman, P., Bylund, G.O., Ganai, R.A., Lundström, E.-B., Sauer-Eriksson, A.E. and Johansson, E. (2014) Structural basis for processive DNA synthesis by yeast DNA polymerase ϵ . *Nat. Struct. Mol. Biol.*, **21**, 49–55.
 96. Baris, Y., Taylor, M.R.G., Aria, V. and Yeeles, J.T.P. (2022) Fast and efficient DNA replication with purified human proteins. *Nature*, **606**, 204–210.
 97. Lancey, C., Tehseen, M., Raducanu, V.-S., Rashid, F., Merino, N., Ragan, T.J., Savva, C.G., Zaher, M.S., Shirbini, A., Blanco, F.J. et al. (2020) Structure of the processive human pol δ holoenzyme. *Nat. Commun.*, **11**, 1109.
 98. Zheng, F., Georgescu, R.E., Li, H. and O'Donnell, M.E. (2020) Structure of eukaryotic DNA polymerase δ bound to the PCNA clamp while encircling DNA. *Proc. Natl. Acad. Sci. U.S.A.*, **117**, 30344–30353.
 99. Smith, D.J. and Whitehouse, I. (2012) Intrinsic coupling of lagging-strand synthesis to chromatin assembly. *Nature*, **483**, 434–438.
 100. Daigaku, Y., Keszthelyi, A., Müller, C.A., Miyabe, I., Brooks, T., Retkute, R., Hubank, M., Nieduszynski, C.A. and Carr, A.M. (2015) A global profile of replicative polymerase usage. *Nat. Struct. Mol. Biol.*, **22**, 192–198.

101. Evrin,C., Maman,J.D., Diamante,A., Pellegrini,L. and Labib,K. (2018) Histone H2A–H2B binding by Pol α in the eukaryotic replisome contributes to the maintenance of repressive chromatin. *EMBO J.*, **19**, e99021.
102. Li,Z., Hua,X., Serra-Cardona,A., Xu,X., Gan,S., Zhou,H., Yang,W.-S., Chen,C., Xu,R.-M. and Zhang,Z. (2020) DNA polymerase α interacts with H3–H4 and facilitates the transfer of parental histones to lagging strands. *Sci. Adv.*, **6**, eabb5820.
103. Gan,H., Serra-Cardona,A., Hua,X., Zhou,H., Labib,K., Yu,C. and Zhang,Z. (2018) The Mcm2-Ctf4-pola axis facilitates parental histone H3–H4 transfer to lagging strands. *Mol. Cell*, **72**, 140–151.